STATE OF THE CLIMATE IN 2010

J. Blunden, D. S. Arndt, and M. O. Baringer, Eds.

Associate Eds. K. M. Willett, A. J. Dolman, B. D. Hall, P. W. Thorne, J. M. Levy, H. J. Diamond, J. Richter-Menge, M. Jeffries, R. L. Fogt, L. A. Vincent, and J. M. Renwick

Special Supplement to the
Bulletin of the American Meteorological Society
Vol. 92, No. 6, June 2011

4. THE TROPICS—H. J. Diamond, Ed.

a. Overview—H. J. Diamond

The year was characterized by a strong El Niño at the beginning of the year, followed by a transition to La Niña conditions in the middle part of the year, and then finally to a moderate-to-strong La Niña by the end of the year. By November, the equatorial cold tongue had intensified significantly, and the Oceanic Niño Index (ONI) dropped to -1.4°C, as the area of sea surface temperature (SST) anomalies colder than -1.0°C expanded westward to cover the entire central and east-central equatorial Pacific.

Overall, global tropical cyclone (TC) activity during 2010 was well-below average, with the lowest number of named storms globally (70) in the last 33 years. Only one basin, the North Atlantic, experienced above-normal activity. This was also the most active season, and the only hyperactive season, on record in the North Atlantic to have no hurricane landfalls in the United States. On the other hand, eastern Canada experienced one of its most active TC seasons on record, as documented in Sidebar 4.1.

This chapter consists of seven sections: (1) El Niño-Southern Oscillation (ENSO) and the Tropical Pacific; (2) Tropical Intraseasonal Activity; (3) seasonal TC activity in the seven TC basins: the North Atlantic, Eastern North Pacific, Western North Pacific, North Indian and South Indian Oceans, Southwest Pacific, and Australia; (4) Tropical Cyclone Heat Potential, which aids in summarizing the section for TCs from an ocean heat perspective; (5) Intertropical Convergence Zone (ITCZ) behavior in the Pacific and Atlantic basins; and (6) the Indian Ocean Dipole (IOD). A new section detailing the Atlantic Multidecadal Oscillation (AMO) has been added to complement some of the other work related to ENSO, the IOD, and the Madden-Julian Oscillation (MJO).

b. ENSO and the Tropical Pacific—G. D. Bell, M. Halpert, and M. L'Heureux

1) Oceanic Conditions

El Niño and La Niña represent opposite phases of the El Niño-Southern Oscillation (ENSO), a coupled ocean-atmosphere phenomenon centered in the equatorial Pacific Ocean. NOAA's Climate Prediction Center (CPC) classifies El Niño and La Niña episodes using the Niño-3.4 index, which reflects area-averaged sea surface temperature (SST) anomalies in the east-central equatorial Pacific between 5°N–5°S and 170°W–120°W.

For historical purposes, the CPC classifies an El Niño (La Niña) episode when the three-month running mean value of the Niño-3.4 index (called the Oceanic Niño Index, ONI) is greater (less) than or equal to +0.5°C (-0.5°C) for five consecutive overlapping months. A time series of the Niño-3.4 index indicates that both El Niño and La Niña occurred during 2010 (Fig. 4.1), with El Niño during January–April and La Niña from July through the end of the year.

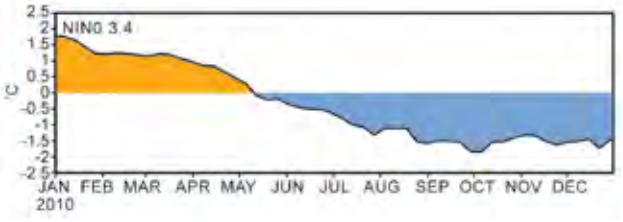

Fig. 4.1. Time series of weekly sea surface temperature anomalies (°C) in the Niño-3.4 region (5°N–5°S, 170°–120°W). Anomalies are departures from the 1971–2000 weekly adjusted OISST climatology of Smith and Reynolds (1998).

A strong El Niño[1] was present during December 2009–February 2010 (DJF), as indicated by an ONI of +1.7°C. During this period, exceptionally warm SSTs (≥ 29°C) extended across the east-central equatorial Pacific, and the warmest SSTs in the entire Pacific basin were located east of the International Date Line (hereafter date line) instead of in their normal position north of Papua New Guinea (Fig. 4.2a). Equatorial SST anomalies during this period exceeded +1°C across most of the Pacific Ocean east of the date line (Fig. 4.2b). During March–May (MAM), El Niño became a weak event as the region of warmest SSTs retracted to well west of the date line (Fig. 4.2c) and the SST anomalies decreased across the eastern half of the equatorial Pacific (Fig. 4.2d).

During June–August (JJA), the equatorial Pacific continued to cool east of the date line, and an anomalously strong cold tongue became established (Figs. 4.2e,f). The resulting SST anomalies reflected the development of a weak La Niña[2], as the ONI dropped to -0.6°C. During September–November (SON), La Niña was a moderate-strength event as the ONI dropped to -1.4°C and the equatorial cold tongue intensified and expanded westward (Fig. 4.2g). The area of SST anomalies colder than -1.0°C also expanded

[1] The CPC unofficially uses an ONI ≥ +1.5°C to classify a strong El Niño. They classify a moderate strength El Niño by an ONI of +1.0°C to +1.4°C, and a weak El Niño by an ONI of +0.5°C to +0.9°C.

[2] CPC unofficially classifies a weak La Niña by an ONI of -0.5°C to -0.9°C, and a moderate strength La Niña by an ONI of -1.0°C to -1.4°C. A strong La Niña is unofficially classified by an ONI ≤ -1.5°C.

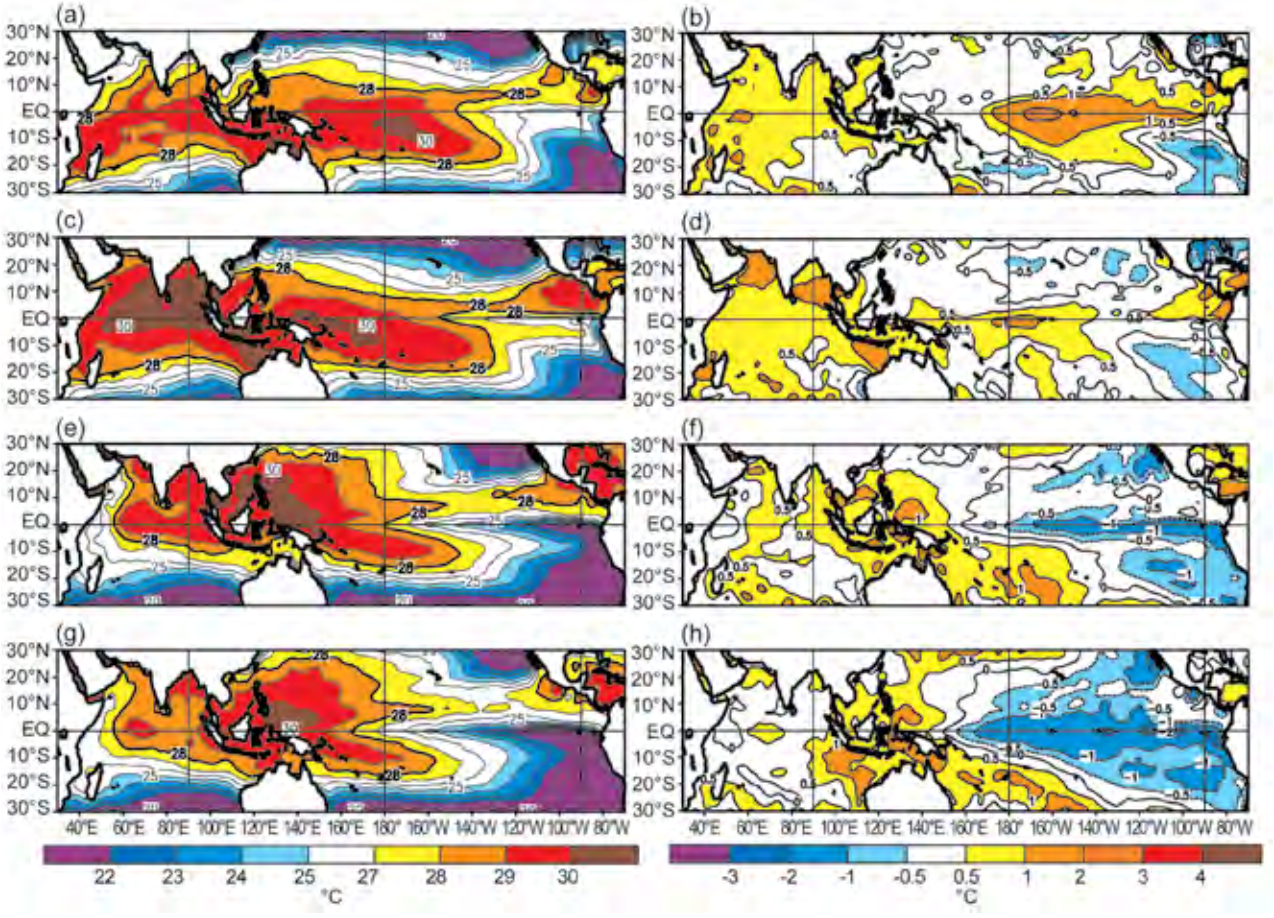

Fig 4.2. Seasonal SST (Left) and anomaly (right) for (a, b) DJF 2009/10, (c, d) MAM 2010, (e, f) JJA 2010 and (g, h) SON 2010. Contour interval for total (anomalous) SST is 1°C (0.5°C). Anomalies are departures from the 1971–2000 seasonal adjusted OISST climatology of Smith and Reynolds (1998).

westward to cover the entire central and east-central equatorial Pacific (Fig. 4.2h).

The subsurface thermal structure is a critical feature of ENSO. As seen during DJF, El Niño featured a deep layer of anomalously warm ocean temperatures east of the date line (Fig. 4.3a), in association with a deeper-than-average thermocline in the central and eastern equatorial Pacific. During MAM, the total volume of anomalously warm water decreased substantially across the eastern half of the equatorial Pacific and the anomalously warm water became confined to the near surface (Fig. 4.3b). This evolution reflected a shoaling of the oceanic thermocline and signified the imminent demise of El Niño.

During JJA and SON, the subsurface thermal structure reflected a markedly increased east-west slope of the oceanic thermocline, which is consistent with La Niña's formation and intensification (Figs. 4.3c,d). This structure reflected a shallower-than-normal thermocline and a deep layer of negative subsurface temperature anomalies in the east-central and eastern Pacific. It also reflected a deeper-than-normal thermocline and positive subsurface temperature anomalies in the western Pacific. By SON, the thermocline in the eastern Pacific had reached the surface and was approximately 120 m shallower than observed earlier in the year in association with El Niño.

2) Atmospheric Circulation: Tropics

El Niño and La Niña both impacted the atmospheric circulation and patterns of tropical convection during 2010, in a manner consistent with past episodes (Chelliah and Bell 2004). As seen during DJF, a key atmospheric component of El Niño is a reduced strength of the normal tropical easterly trade winds (i.e., westerly anomalies) east of the date line (Fig. 4.4a). This wind pattern contributed to a reduction in upwelling and to an anomalous eastward transport of warm water from the western Pacific, both of which strengthened El Niño.

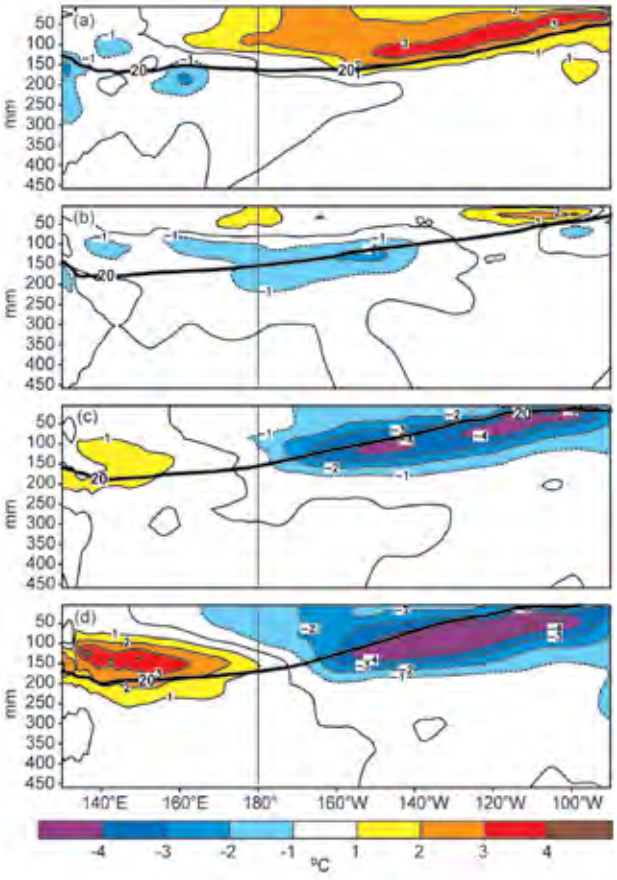

Fig 4.3. Equatorial depth-longitude section of ocean temperature anomalies (°C) averaged between 5°N and 5°S during (a) DJF 2009/10, (b) MAM 2010, (c) JJA 2010, and (d) SON 2010. The 20°C isotherm (thick solid line) approximates the center of the oceanic thermocline. The data are derived from an analysis system that assimilates oceanic observations into an oceanic global circulation model (Behringer et al. 1998). Anomalies are departures from the 1971–2000 period monthly means.

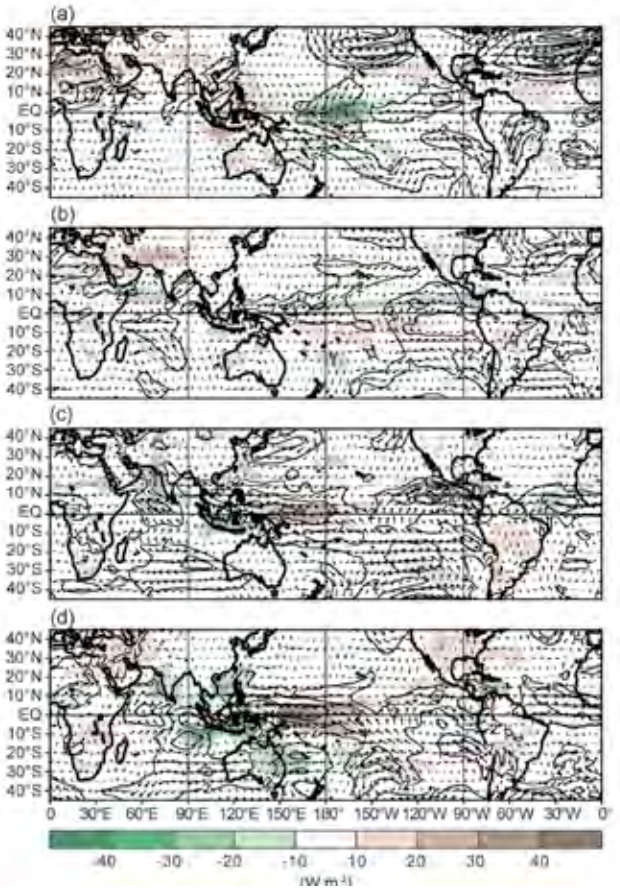

Fig. 4.4. Anomalous 850-hPa wind vector and speed (contours, m s^{-1}) and anomalous outgoing longwave radiation (shaded, W m^{-2}) during (a) DJF 2009/10, (b) MAM 2010, (c) JJA 2010, and (d) SON 2010. Anomalies are departures from the 1979–95 period monthly means.

During this period, convection was enhanced (green shading) over the central and east-central equatorial Pacific, and suppressed (brown shading) over the western Pacific and Indonesia. At 200 hPa, these conditions resulted in anticyclonic circulation anomalies in the subtropics of both hemispheres flanking the region of enhanced convection, and cyclonic circulation anomalies in both hemispheres flanking the region of suppressed convection (Fig. 4.5a). Collectively, the above conditions reflect a weakening of the equatorial Walker circulation, along with an anomalously weak (strong) Hadley circulation over the western (central) Pacific.

El Niño's weakening during MAM was associated with two main changes in the low-level winds (Fig. 4.4b). First, the trade winds became enhanced west of the date line, which acted to transport exceptionally warm water toward the western Pacific. Second, an anomalously strong cross-equatorial flow became established over the east-central equatorial Pacific, which resulted in increased upwelling and cooler sea surface and subsurface temperatures in that region.

La Niña's development and intensification during JJA and SON was associated with a further strengthening of the anomalous easterly trade winds across the western tropical Pacific and with an expansion in the area of anomalous cross-equatorial flow to cover the entire eastern half of the equatorial Pacific (Figs. 4.4c,d). Consistent with this evolution, equatorial convection became suppressed across a large area west of the date line, and enhanced over Indonesia and the eastern Indian Ocean. These conditions are typical of La Niña and reflected an enhanced equatorial Walker circulation and a suppressed Hadley circulation over the central Pacific.

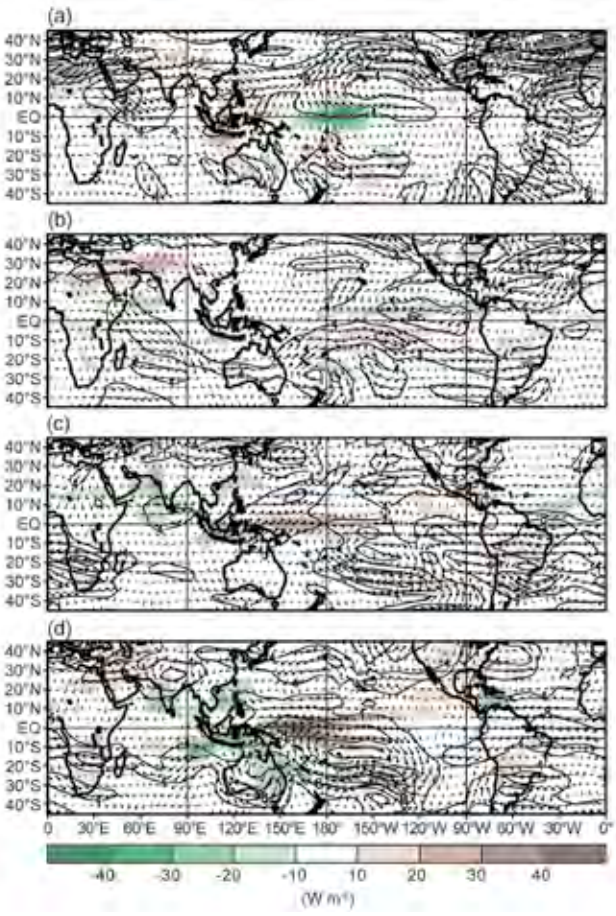

Fig. 4.5. Anomalous 200-hPa wind vector and speed (contours, m s^{-1}) and anomalous outgoing longwave radiation (shaded, W m^{-2}) during (a) DJF 2009/10, (b) MAM 2010, (c) JJA 2010, and (d) SON 2010. Anomalies are departures from the 1979–95 period monthly means.

As a result, La Niña impacts on the upper-level circulation were seen across the tropical and subtropical Pacific in both seasons (Figs. 4.5c,d). These impacts included the development and strengthening of cyclonic circulation anomalies in the subtropics of both hemispheres, in association with the region of suppressed convection. In both seasons, the resulting downstream easterly wind anomalies extended across the eastern North Pacific and Caribbean Sea, which acted to: (1) reduce the vertical wind shear and enhance the Atlantic hurricane season (section 4d2) and (2) increase the vertical wind shear and suppress hurricane activity in both the Central and Eastern North Pacific hurricane basins (section 4d3).

3) Atmospheric Circulation: Extratropics

As seen during DJF, El Niño was associated with an eastward extension of deep tropical convection and deep tropospheric heating to well east of the date line, resulting in an eastward extension of the subtropical ridges in both hemispheres. The wintertime East Asian jet stream, which is intrinsically linked to the poleward flank of the subtropical ridge, also extended eastward to span the entire Pacific basin. Likewise, the associated jet exit region (and therefore the main cyclogenesis region) shifted eastward to the area immediately upstream of the southwestern U.S. (Fig. 4.6, shading).

These observations highlight key jet-like features of the El Niño-related anomalous anticyclonic circulation over the east-central Pacific. These features include: (1) an anomalous westerly jet core along its northern flank (near 30°N between the date line and the western U.S.), which coincides with the observed East Asian jet axis; (2) anomalous southwesterly winds and speed acceleration (solid contours) along its western flank near the date line, which represent the anomalous jet entrance region; and (3) anomalous northwesterly winds and speed deceleration (dashed contours) along its eastern flank over the eastern Pacific, which capture the anomalous jet exit region.

Consistent with the above conditions, the Pacific storm track was shifted well south and east of normal during DJF, resulting in increased storminess and above-average precipitation across the southern U.S. Also, the 500-hPa Hudson Bay trough was weaker than average and the trough over the southeastern U.S. was stronger than average (see Fig. 8.2). As a result, a more zonally-uniform distribution of both temperature and winds, which is characteristic of El Niño, prevailed across the Pacific basin and much of North America.

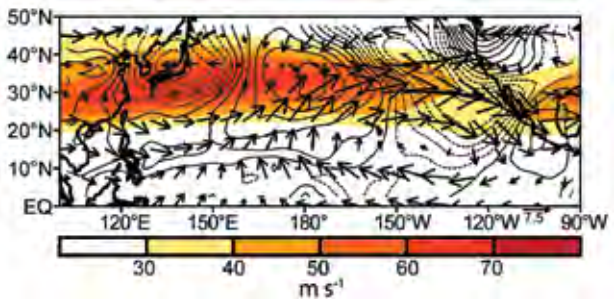

Fig. 4.6. DJF 2009/10: Total 200-hPa wind speed (m s^{-1}, shaded), anomalous wind vector, and anomalous horizontal wind speed tendency (d/dt) (contours, interval is 1 x 10^{-4} m s^{-2}). Solid (dashed) contours show anomalous speed acceleration (deceleration), where

$$dV_a/dt = (-V \cdot \nabla Z) - (-V_c \cdot \nabla Z_c)$$

where V is the observed total vector wind, Z is the observed total geopotential height, and the subscript "c" denotes the climatological mean values. Anomalies are departures from the 1971–2000 period monthly means. Vector scale is shown at bottom right.

Later in the year, La Niña affected the extratropical circulation over the South Pacific basin. For example, the cyclonic anomalies over the central subtropical South Pacific during SON reflected a strengthening of the normal mid-Pacific trough, and a westward retraction of the subtropical ridge axis to the extreme western Pacific (Fig. 4.5d). These conditions were associated with easterly 200-hPa wind anomalies across the central Pacific near 30°S, which coincided with the exit region of the South Pacific jet core and therefore reflected a weakening and westward retraction of that jet to west of the date line.

4) ENSO Temperature and Precipitation Impacts

During DJF 2009/10, the precipitation patterns typically associated with El Niño (Ropelewski and Halpert 1987) were observed over parts of the world. These included above-average precipitation over the central equatorial Pacific, the southern U.S., southeastern South America, and equatorial eastern Africa (see Fig. 8.1). They also included below-average precipitation over Indonesia, parts of the Amazon Basin, and southeastern Africa.

Typical El Niño-related temperature impacts during DJF included warmer-than-average conditions over southeastern Asia, Canada, and southeastern Brazil, and cooler-than-average conditions across the southern United States. In the U.S., the temperature and precipitation patterns were also modulated by a strong negative phase of the Arctic Oscillation (AO) and North Atlantic Oscillation (NAO), which favored exceptionally cool conditions across much of the country and contributed to a series of heavy snowfall events along the east coast (see section 7b2 and Sidebar 7.1 for more details).

La Niña impacted global precipitation patterns during JJA and SON in a manner consistent with past cold episodes (Ropelewski and Halpert 1989). These impacts included suppressed convection across the central equatorial Pacific, coupled with above-average rainfall across much of the Maritime Continent (Indonesia, Philippines, Malaysia, and Borneo). La Niña impacts during SON also included below-average precipitation in southeastern South America, and above-average rainfall across eastern Australia (see Fig. 8.7).

c. Tropical Intraseasonal Activity—J. Gottschalck, G. D. Bell, and S. Weaver

The Madden-Julian Oscillation (MJO) (Madden and Julian 1971, 1972, 1994) is a leading climate mode of tropical convective variability that occurs on intraseasonal timescales. The convective anomalies associated with the MJO often have the same spatial scale as ENSO, but differ in that they exhibit a distinct eastward propagation. If the MJO remains active, convective anomalies at a given location repeat approximately every 30–60 days on average. The MJO can strongly affect the tropical and extratropical atmospheric circulation patterns, and may produce short-lived ENSO-like convective anomalies across the tropics (Mo and Kousky 1993; Kousky and Kayano 1994; Kayano and Kousky 1999) .The MJO is often quite variable in a given year, with periods of moderate-to-strong activity sometimes followed by little or no activity. Overall, the MJO tends to be most active during neutral and weak ENSO periods, and is often absent during strong El Niño events (Hendon et al. 1999; Zhang and Gottschalck 2002; Zhang 2005).

The MJO is seen by continuous eastward propagation of 200-hPa velocity potential anomalies around

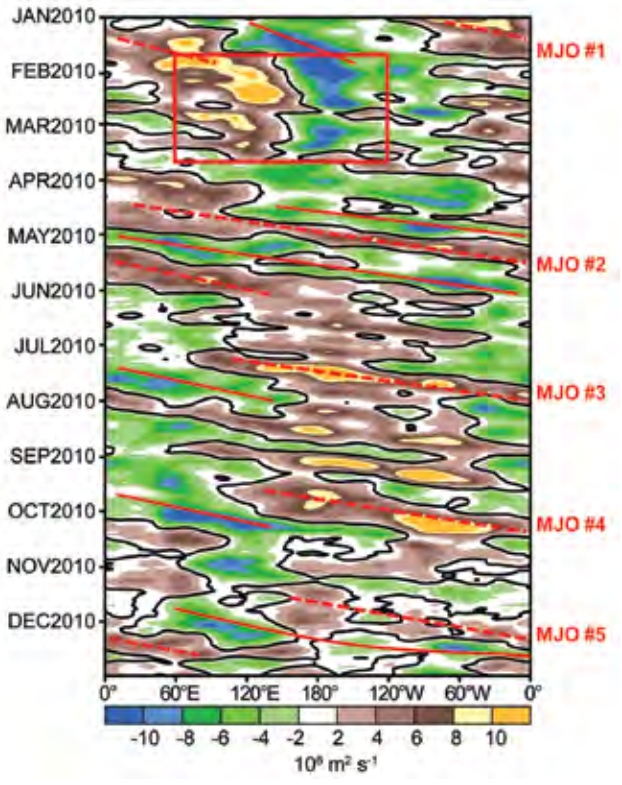

Fig. 4.7. Time-longitude section for 2010 of anomalous 200-hPa velocity potential (x 10^6 m^2 s^{-1}) averaged between 5°N and 5°S. For each day, the period mean is removed prior to plotting. Green (brown) shading highlights likely areas of anomalous divergence and rising motion (convergence and sinking motion). Red lines and labels highlight the main Madden Julian Oscillation episodes. Anomalies are departures from the 1971–2000 base period daily means.

the globe. A time-longitude section of this parameter shows five MJO episodes during 2010 (Fig. 4.7). These include: (1) a strong episode that continued from late 2009 into early February 2010 (MJO #1); (2) a moderate-strength episode with higher frequency during April and May (MJO #2); (3) a moderate-strength but short-lived episode during July and also during September–October (MJO #3 and #4); and (4) a generally weak and short-lived episode during mid-November to mid-December (MJO #5).

The first MJO (MJO #1) featured strong convective anomalies that propagated eastward and became in phase with those associated with El Niño. The observations suggest that this evolution likely aided the development of more persistent and stationary El Niño-related convective anomalies during late January through early March, as highlighted in the red box in Fig. 4.7 by suppressed convection over Indonesia and enhanced convection near the date line. Prior to this, the El Niño-related enhanced convection was more sporadic over the central equatorial Pacific.

Also associated with MJO #1 were strong low-level westerly wind anomalies (not shown) within and to the rear of the main area of enhanced convection. The resulting westerly wind burst triggered a downwelling oceanic Kelvin wave (Fig. 4.8, dashed line). This wave formed over the western equatorial Pacific in late January and reached the South American coast in late March and early April. Oceanic warming associated with this wave likely contributed to the apparent intensification of El Niño. This was the only appreciable downwelling oceanic Kelvin wave of the year.

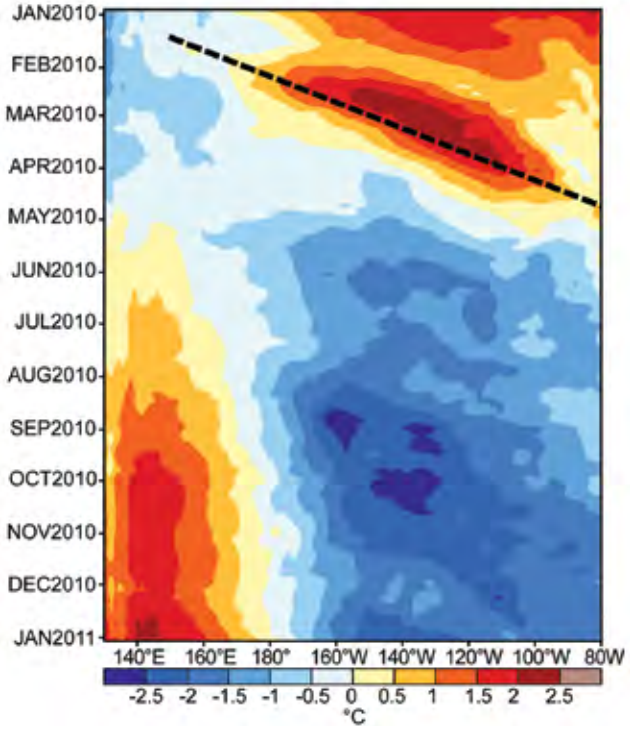

Fig 4.8. Time-longitude section for 2010 of the anomalous upper ocean (0 m–300 m) heat content averaged between 5°N and 5°S. Blue (yellow/red) shading indicates below (above) average heat content. The downwelling phases (dashed lines) of equatorial oceanic Kelvin waves are indicated. Anomalies are departures from the 1982–2004 base period pentad means.

The moderate-strength MJO activity during April and May (MJO #2) had a shorter periodicity (approximately 30 days) than that observed earlier in the year. Short-lived, moderate-strength MJO activity was also observed during July (MJO #3). Following this event, the intraseasonal variability during August and much of September primarily reflected higher frequency atmospheric Kelvin wave activity (Wheeler and Kiladis 1999; Wheeler and Weickmann 2001).

The two remaining MJO events (MJO #4 and #5) were characterized by enhanced convection that was primarily limited to Indonesia and to the western Pacific across the South Pacific Convergence Zone (SPCZ). This off-equatorial displacement of the convective anomalies was primarily a result of La Niña, which contributed to above-average sea surface temperatures in the SPCZ region and to much-below-normal sea surface temperatures across the equatorial Pacific Ocean.

d. Tropical Cyclones

1) Overview—H. J. Diamond and B. C. Trewin

The global tallying of total tropical cyclone (TC) numbers is challenging and involves more than simply adding up basin totals because some storms cross basin boundaries, some basins overlap, and multiple agencies are involved in tracking and forecasting TCs. Compiling the activity over all seven TC basins, the 2010 season (2009/10 in the Southern Hemisphere) saw a well-below-normal (1981–2009 base) number of named storms [NS; wind speeds ≥ 34 kts (17.5 m s^{-1})] and a below-average number of hurricanes/typhoons/cyclones [HTC; ≥ 64 kts (32.9 m s^{-1})] and major HTCs [≥ 96 kts (49.4 m s^{-1})]. Globally, 70 named storms[3] developed during the 2010 season (global average is 86.5), with 42 becoming HTCs (global average is 45.4). Of these, 22 (compared to 26 in 2006, 18 in 2007, 20 in 2008, and 16 in 2009) attained major/intense status

[3] It should be noted that in the Western North Pacific there were an additional five unnamed tropical depressions recorded by the Japan Meteorological Agency that were not included in this total.

(global average is 21.9). Therefore, while overall NS count was well-below average, the number of major/intense storms was near the global average[4].

Globally, the 2009/10 season featured the fewest number of NSs since the 2006/07 season (84). However, while the total number of NSs was less than the 2006/07 season, it is interesting to note that the total number of HTCs (42) was nearly the same as in 2006/07 (43). Historically, NS records are incomplete in all basins, especially prior to the beginning of reasonably comprehensive satellite coverage around 1970. Based on the International Best Tracks Archive for Climate Stewardship (IBTrACS) dataset (Knapp et al. 2010), the 2009/10 global NS total was the third lowest since 1970 and only slightly above the record low of 63 NSs observed during the 1976/77 season. Focusing only on the January–December calendar year, 2010 featured the lowest number of NSs (67) since 1970. The previous record-low NS activity in any calendar year was 68, observed in both 1976 and 1977.

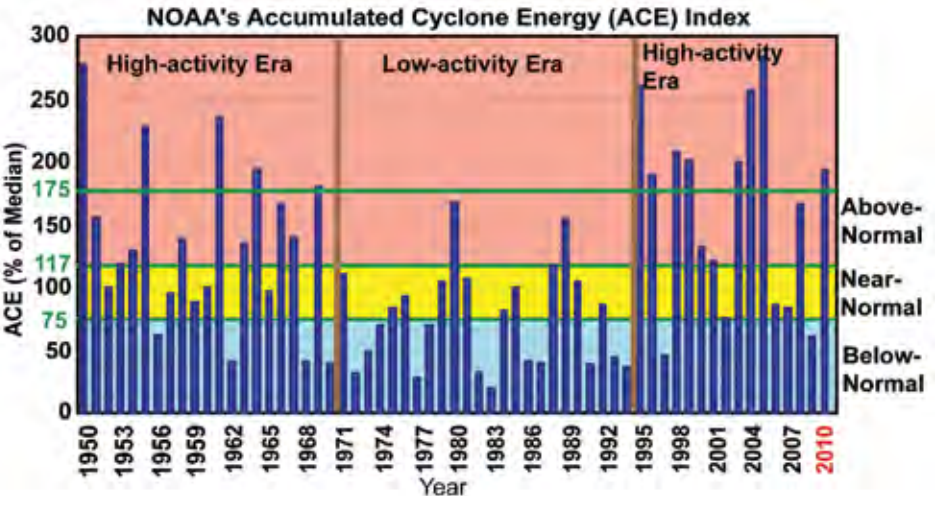

Fig. 4.9. NOAA's Accumulated Cyclone Energy (ACE) Index in the Atlantic Basin expressed as percent of the 1950–2000 median value (87.5 x 10^4 kt^2). The ACE is a wind energy index that measures the combined strength and duration of the named storms. ACE is calculated by summing the squares of the six-hourly maximum sustained wind speed (measured in knots) for all periods while the named storm has at least tropical storm strength. Pink, yellow, and blue shadings correspond to NOAA's classifications for above-, near- and below-normal seasons, respectively. The 175% threshold for a hyperactive season is indicated. Vertical brown lines separate high-activity and low-activity eras.

The 2009/10 seasonal total of 70 TCs thus nearly equals the most inactive season globally since 1976/77 when there were 63 storms globally. No year in recent times has approached the 2010 seasonal low; the last sub-75 storm season was 1987/88 (73), and the last sub-80 storm season was 1994/95 (78). It was a particularly exceptional record-low season in the North Pacific. The northwest Pacific had its most inactive year since satellite records began, while the northeast Pacific equaled its record low. The 22 named storms across the two basins were less than half the usual number in what are normally the world's most active tropical cyclone regions. Activity in the North and South Indian Ocean was also substantially below normal, while the southwest Pacific was close to normal. Conversely, the Atlantic basin produced 19 NSs, well exceeding the long-term average of 11. In the southwest Pacific, NS activity during 2010 was near normal. However, the latter part of the hurricane season in this region was extremely active, producing three Category 4 TCs and one Category 5 TC. These storms resulted in a total of 14 fatalities and produced a minimum estimated damage of $163 million (U.S. dollars). Scaling these numbers for a region as sparsely populated and undeveloped as the southwest Pacific, these are actually very large totals.

2) Atlantic Basin—G. D. Bell, E. S. Blake, T. B. Kimberlain, C. W. Landsea, J. Schemm, R. J. Pasch, and S. B. Goldenberg

(i) 2010 Seasonal Activity

The official Atlantic hurricane season lasts from June through November, with August–October (ASO) typically being the peak months of the season. The 2010 Atlantic hurricane season produced 19 NSs, of which 12 became hurricanes and 5 became major hurricanes. All but two NSs formed during ASO. The 1950–2000 seasonal averages are 11 named storms[5],

[4] Global averages are calculated from the International Best Tracks Archive for Climate Stewardship dataset at http://www.ncdc.noaa.gov/oa/ibtracs/.

[5] Landsea et al. (2010) indicate that because of improved monitoring and analysis of weak, short-lived tropical cyclones in the last decade, the climatological averages since 1950 may be biased low by about two tropical storms per year, giving a more realistic climatology value of about 13 named storms per year.

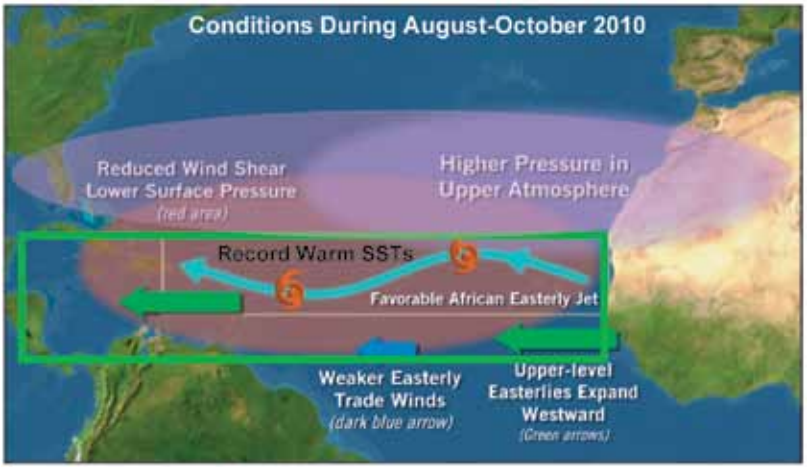

Fig. 4.10. Schematic depiction of atmospheric and oceanic conditions over the Atlantic basin during August–October 2010. Green box denotes the Main Development Region (MDR).

six hurricanes, and two major hurricanes. The IBTrACS 1980–2009 seasonal averages are 12.2 NSs, 6.6 hurricanes, and 2.7 major hurricanes.

The 2010 seasonal Accumulated Cyclone Energy (ACE) value (Bell et al. 2000) was 166.3 x 10^4 kt^2, which corresponds to 190% of the 1950–2000 median value (Fig. 4.9). This places 2010 as the 10th most active season since 1950. This year also marks the ninth hyperactive season (ACE ≥ 175% of the median) since the high activity era for Atlantic hurricanes began in 1995 (Goldenberg et al. 2001). By comparison, no hyperactive seasons occurred during the preceding 24-year period (1971–94), which is a low activity era in the Atlantic Basin.

As is typical of very active seasons, conditions for tropical cyclone formation and intensification during 2010 were exceptionally conducive within the Main Development Region (MDR), which encompasses the Caribbean Sea and tropical Atlantic Ocean between 9.5°N and 21.5°N (Fig. 4.10). Most (14 of 19) named storms formed in the MDR, accounting for 10 of 12 hurricanes, all five major hurricanes, and 93% of the seasonal ACE value.

(ii) Storm Tracks and Landfalls

The Atlantic storm tracks during 2010 were generally divided into two clusters. One cluster comprised eight storms that formed over the eastern tropical Atlantic. Five of these eventually became hurricanes (four became major hurricanes) and three remained tropical storms. The majority of these storms (six of eight) tracked northwestward and then recurved out to sea. Two (Earl and Igor) struck Nova Scotia and Newfoundland, respectively (see Sidebar 4.1 for more detailed information on the 2010 Atlantic hurricane season impacts on Canada). This landfall ratio (25%) is close to the historical probability (29%) for a North America landfall by storms forming over the eastern Atlantic (Kossin et al. 2010).

The second cluster of storm tracks consisted of 11 systems that formed over or near the Caribbean Sea. This region typically sees significantly increased hurricane activity during hyperactive seasons. Many of

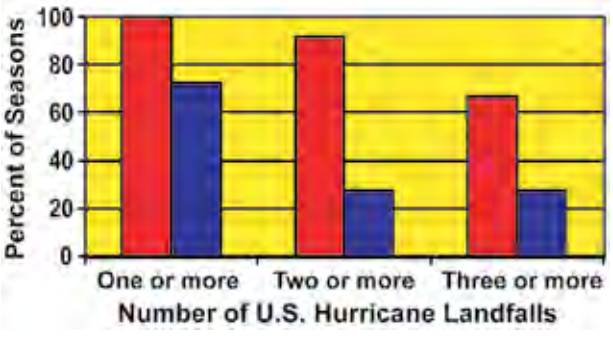

Fig. 4.11. Seasonal frequency of Atlantic basin hurricanes making landfall in the United States (during 1950–2009) for hyperactive seasons (red bars) and for above-normal seasons that are not hyperactive (blue bars). Landfalls are based on the HURDAT data produced by the National Hurricane Center and compiled by Blake et al. (2007). Only one U.S. hurricane landfall per storm is counted.

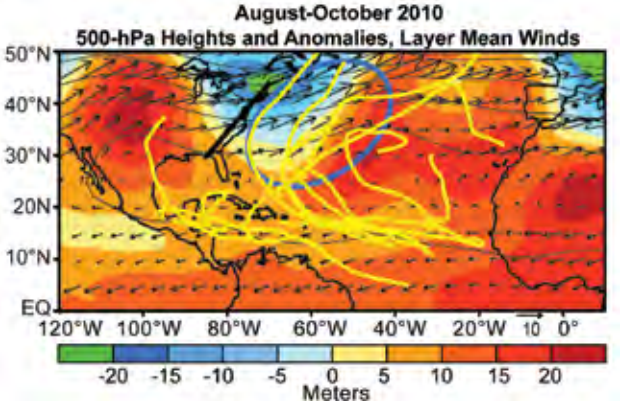

Fig. 4.12. Map of August–October 2010 500-hPa heights (contours, m) and anomalies (shading), and layer mean vector wind (m s^{-1}) between 600 hPa and 300 hPa. Vector scale is located at bottom right. Thick solid line indicates weakness in upper-level ridge and blue circle indicates extensive southwesterly flow over the western Atlantic. August–October 2010 Atlantic named storm tracks are shown in yellow.

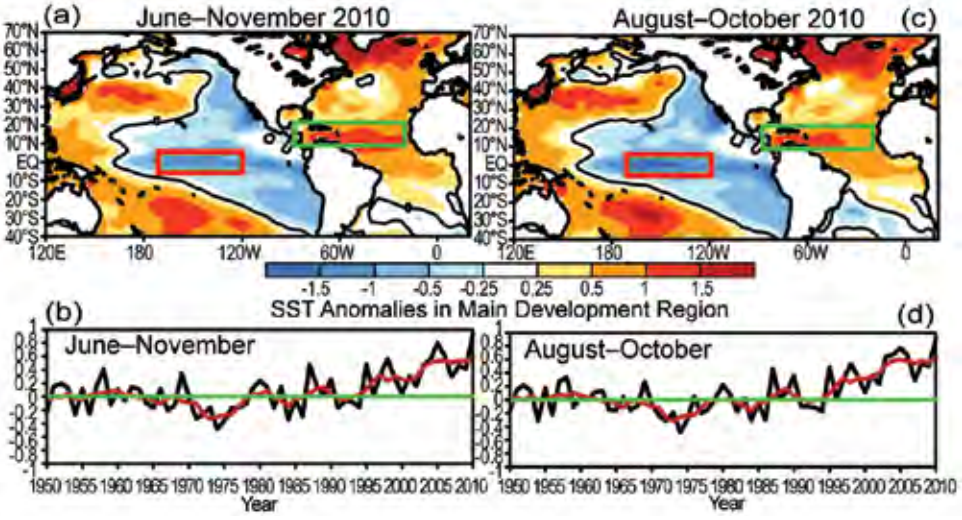

Fig. 4.13. (Top) Sea surface temperature (SST) anomalies (°C) during (a) June–November 2010 and (c) August–October 2010. (Bottom) Time series of consecutive area-averaged SST anomalies in the Main Development Region (MDR) during (b) June–November, and (d) August–October. Red line shows the corresponding five-year running mean. Green boxes in (a) and (c) denote the MDR. Anomalies are departures from the ERSST-V3b (Smith et al. 2008) 1971–2000 period monthly means.

these storms during 2010 formed near land over the western Caribbean/Mexico/Central America region. Five systems in this second cluster made landfall as tropical storms, three made landfall as Category 1–2 hurricanes, and one made landfall as a major hurricane (Category 3–5). It is atypical for above-normal seasons to have no NSs in the northern Gulf of Mexico. However, no NSs tracked over this region during 2010, meaning minimal adverse affects on the oil well capping and associated cleanup efforts associated with the Deepwater Horizon accident.

The U.S. also did not experience any landfalling hurricanes during 2010. This was the most active season—and the only hyperactive season—on record with no U.S. hurricane landfalls. For the 12 hyperactive seasons that occurred during 1950–2009, each produced at least one U.S. landfalling hurricane and 90% produced at least two U.S. landfalling hurricanes (Fig. 4.11, red bars). This rate of multiple hurricane landfalls is more than triple that (25%) associated with other above-normal seasons that were not hyperactive (blue bars).

The lack of U.S. hurricane landfalls during 2010 can be attributed to several factors. First, there was a pronounced weakness over the eastern U.S. in the extensive subtropical ridge that otherwise extended from Africa to the southwestern U.S. (Fig. 4.12). This weakness reflected mean troughing near the U.S. East Coast, and was associated with midlevel southwesterly flow that steered all approaching hurricanes away from the United States. Second, no hurricanes formed or tracked over the central and northern Gulf of Mexico, which can be attributed in part to the enhanced subtropical ridge over the Caribbean Sea. This ridge prevented storms over this region from propagating northward into the central Gulf. Third, some storms formed and remained over the extreme eastern tropical Atlantic throughout their life.

(iii) Atlantic sea surface temperatures

Mean sea surface temperatures (SSTs) in the MDR

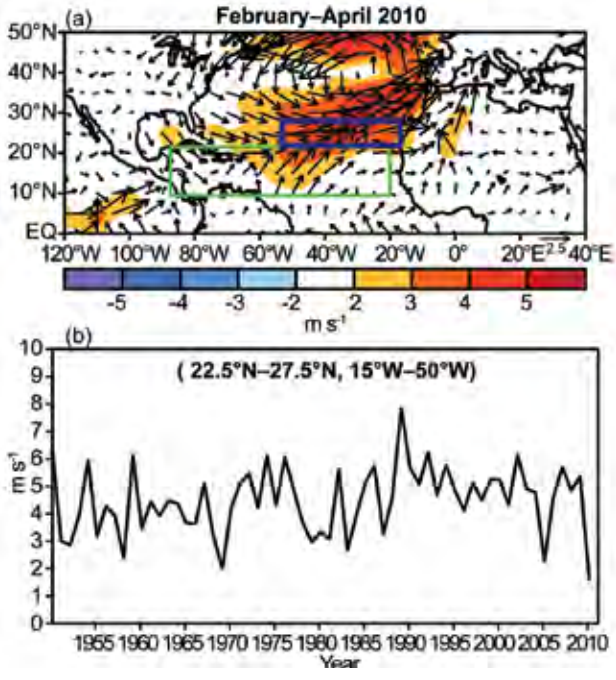

Fig. 4.14. (a) Map of February–April 2010 1000-hPa anomalous wind speed (shaded, m s^{-1}) and vector winds, and (b) time series of consecutive area-averaged total wind speed (m s^{-1}) at 1000 hPa in the area bounded by 22.5°N–27.5°N, 15°W–50°W (blue box in panel a). Green box in (a) denotes the Main Development Region.

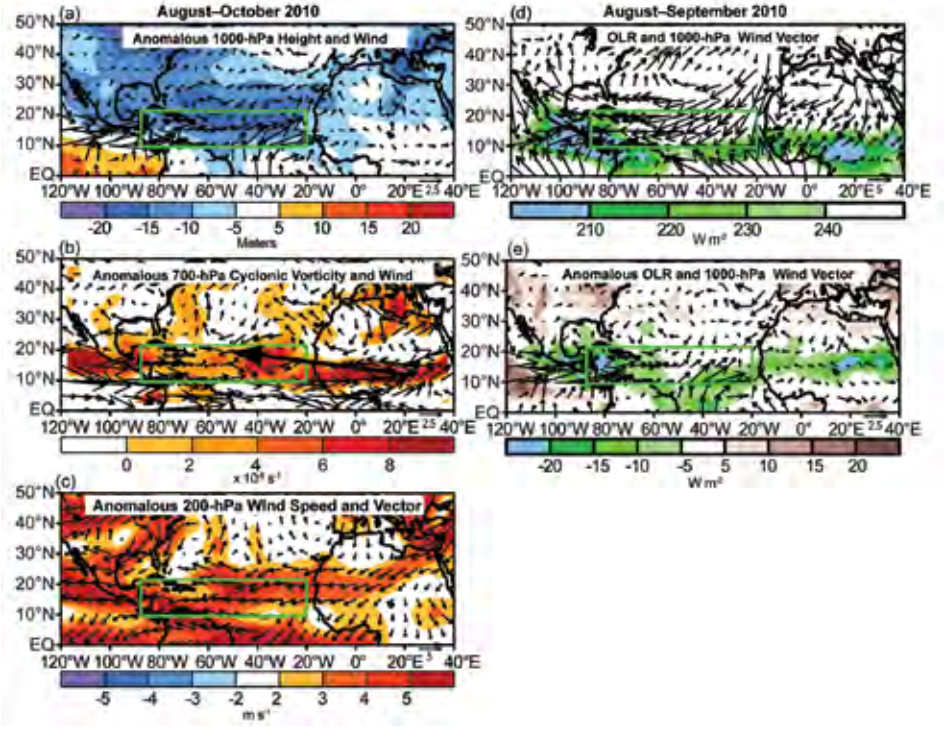

Fig. 4.15. Atmospheric circulation (left) August–October 2010 and (right) August–September 2010: (a) August–October anomalous 1000-hPa height (shading) and vector wind (m s^{-1}), (b) August–October anomalous 700-hPa cyclonic relative vorticity (shading, x 10^{-6} s^{-1}) and vector wind, with thick solid line indicating the axis of the African easterly jet, and (c) August–October anomalous 200-hPa wind speed (shading) and vector wind. Panels (d, e) show August–September conditions: (d) total Outgoing Longwave Radiation (OLR, W m^{-2}) and 1000-hPa vector wind; and (e) August–September anomalous OLR (W m^{-2}) and 1000-hPa anomalous vector wind. Green boxes denote the Main Development Region. Vector scale is at bottom right of each panel. Circulation (OLR) anomalies are with respect to the 1971–2000 period monthly means.

during June–November were 0.93°C above average (Fig. 4.13a). This departure exceeds the previous high (dating back to 1854) of +0.80°C set in 2005 (Fig. 4.13b). The SSTs in the MDR during August–October 2010 were 0.91°C above average (Fig. 4.13c), which also exceeds the previous high August–October departure of +0.77°C set in 2005 (Fig. 4.13d). These record SSTs first appeared during February–April 2010, in association with a pronounced weakening of the anti-cyclonic gyre over the central North Atlantic (Fig. 4.14a) and with unusually weak trade winds north of the MDR (Fig. 4.14b). These conditions were associated with an all-time negative phase of the North Atlantic Oscillation (NAO) during December–April, as measured by the 500 hPa-based NAO index produced by the Climate Prediction Center (CPC; data available at ftp://ftp.cpc.ncep.noaa.gov/wd52dg/data/indices/tele_index.nh). During December–February, this pattern was coupled with a record negative phase of the hemispheric-scale Arctic Oscillation (data available at http://www.cpc.ncep.noaa.gov/products/precip/CWlink/daily_ao_index/monthly.ao.index.b50.current.ascii.table).

The unusually warm SSTs persisted in the MDR through September, as the area of exceptionally weak trade winds subsequently shifted into the deep tropics (Fig. 4.15a). Weaker-than-normal trade winds and anomalously warm SSTs have generally prevailed in the MDR since 1995, in association with the warm phase of the Atlantic Multidecadal Oscillation (AMO; Enfield and Mestas-Nuñez 1999) and active Atlantic phase of the tropical multidecadal signal (Bell and Chelliah 2006; Bell et al. 2009). These conditions have been superimposed upon a weaker long-term warming trend, which some studies suggest is partly linked to anthropogenic greenhouse warming (Santer et al. 2006).

(iv) Atmospheric circulation

Conditions within the MDR reflected an interrelated set of atmospheric anomalies (Fig. 4.10) that are typical of recent active hurricane seasons (Landsea et al. 1998; Bell et al. 1999, 2000, 2004, 2006, 2009; Goldenberg et al. 2001; Bell and Chelliah 2006; Kossin and Vimont 2007). These conditions, combined with La Niña and record warm Atlantic SSTs, set the stage for the 2010 Atlantic hurricane season.

In the lower atmosphere, August–October conditions within the MDR included weaker trade winds, a deep layer of anomalous cross-equatorial flow, and below-average heights/sea-level pressure (Fig. 4.15a,

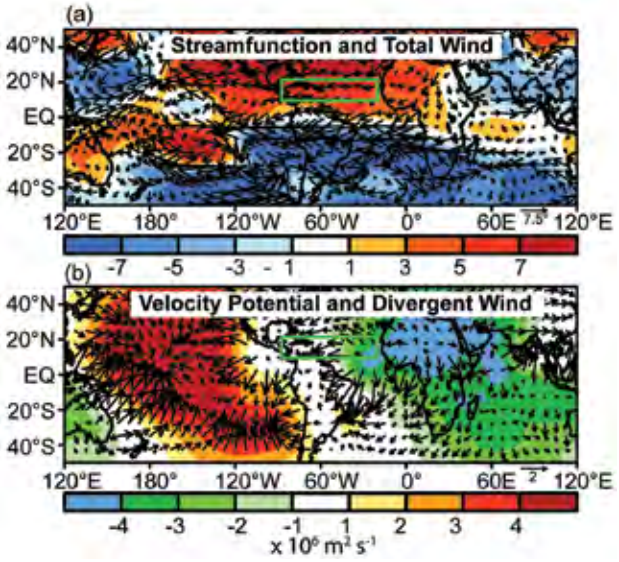

Fig. 4.16. Map of August–October 2010 200-hPa anomalies of (a) streamfunction (shading, x 10^6 m^2 s^{-1}) and vector wind (m s^{-1}) and (b) velocity potential (shading, x 10^6 m^2 s^{-1}) and divergent vector wind (m s^{-1}). Vector scale is at bottom right of each panel. Departures are with respect to the 1971–2000 period. In (a) anomalous ridges are indicated by positive values (red) in the Northern Hemisphere (NH) and negative values (blue) in the Southern Hemisphere (SH). Anomalous troughs are indicated by negative values in the NH and positive values in the SH. Green boxes denote the Main Development Region.

blue shading). Across the Atlantic basin and Sub-Saharan Africa, the low-level westerly anomalies extended above 700 hPa, the approximate level of the African Easterly Jet (AEJ; Fig. 4.15b), and were associated with an anomalous 5° latitude northward shift of the AEJ core (black arrow).

As a result, the bulk of the African easterly wave energy (Reed et al. 1977) was often centered well within the MDR. The AEJ also featured increased cyclonic shear along its equatorward flank within the MDR (Fig. 4.15b, red shading), which dynamically favors stronger easterly waves and an increased cyclonic rotation within which thunderstorms can organize.

An opposite pattern of wind anomalies was evident at 200 hPa, where anomalous easterly flow extended from subtropical central Africa to the eastern North Pacific (Fig. 4.15c). This pattern reflected a stronger and more westward extension of the tropical easterly jet, which occurred in association with an enhanced upper-level ridge that spanned the entire subtropical North Atlantic (Fig. 4.16a).

These conditions were accompanied by a northward shift of the Atlantic Intertropical Convergence Zone (ITCZ), which extended into the southern MDR during August and September (Fig. 4.15d), and resulted in enhanced convection across the region (Fig. 4.15e, green shading). They were also associated with an amplified West African Monsoon system during August–October, as indicated by enhanced convection across the African Sahel and Sudan regions and by a large area of negative velocity potential anomalies over northern Africa (Fig. 4.16b).

Within the MDR, the low-level westerly and upper-easterly anomalies resulted in weak vertical wind shear (less than 8 m s^{-1}) across the entire MDR (Fig. 4.17a). The most anomalously weak shear spanned the central tropical Atlantic and Caribbean Sea (Fig. 4.17b, orange shading), where the total shear was less than 4 m s^{-1}. These conditions were part of a larger-scale pattern that included increased shear across the eastern equatorial Atlantic and over the eastern tropical North Pacific (Fig. 4.17b, blue shading). This pattern is typical of other very active Atlantic hurricane seasons (Bell and Chelliah 2006). At the same time, historically low hurricane activity prevailed across the central and eastern Pacific hurricane basins (see section 4d3).

For the Atlantic basin, the above conditions meant that tropical storms developed primarily within the MDR from amplifying easterly waves moving westward from Africa. These systems quickly entered

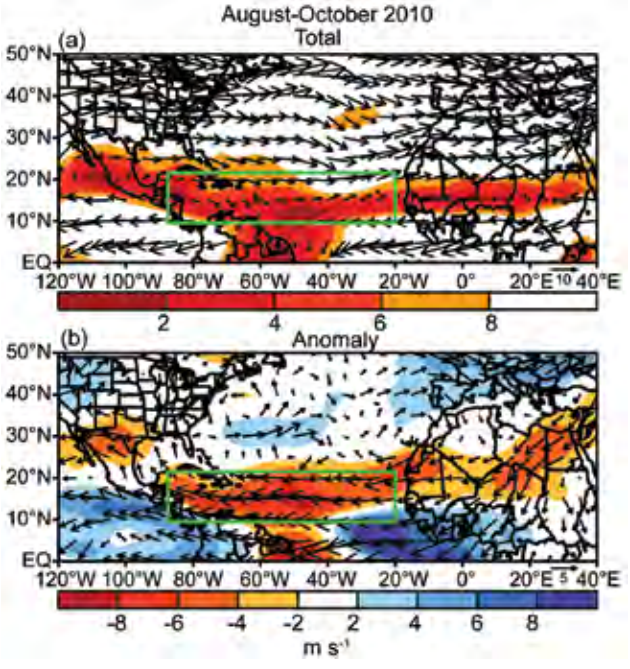

Fig. 4.17. Maps of August–October 2010 (a) total and (b) anomalous vertical wind shear magnitude and vector (m s^{-1}). Vector scale is at bottom right of each panel. Departures are with respect to the 1971–2000 period monthly means.

an extensive area of below-average pressure, deep tropical moisture, increased low-level convergence associated with the ITCZ, and increased cyclonic shear south of the AEJ core. Many of these systems then strengthened while propagating westward within the extended region of very weak vertical wind shear and often over record-warm SSTs. These overall anomaly patterns have favored increased storm formation and intensification since 1995.

(v) Links to Global Climate Patterns

The regional atmospheric conditions during 2010 showed strong links to a combination of three climate factors. The first is the active Atlantic phase of the tropical multidecadal signal, which reflects an interrelated set of conditions that have been conducive to increased Atlantic hurricane activity since 1995 (Bell and Chelliah 2006). The second is La Niña, which contributed to the extensive area of weak vertical wind shear and upper-level easterlies across the MDR. The third is record-warm SSTs in the MDR, as discussed above.

(vi) The Tropical Multidecadal Signal and La Niña

Since 1995, more than two-thirds (11 of 16) of Atlantic hurricane seasons have been above normal and only two have been below normal (Fig. 4.9). This elevated level of activity contrasts sharply with the preceding low-activity era of 1971–94, during which one-half of the seasons were below normal and only three were above normal.

The transition to the current era of high activity was associated with a phase change in the tropical multidecadal signal, which reflects the leading modes of tropical convective rainfall variability and Atlantic SSTs occurring on multidecadal time scales (Bell and Chelliah 2006; Bell et al. 2007). This signal directly links low-frequency atmospheric variability across the central and eastern MDR to an east-west oscillation in anomalous convection between western Africa (Landsea and Gray 1992; Goldenberg and Shapiro 1996) and the Amazon Basin (Fig. 4.16).

All key features of this signal were again present during 2010, suggesting no weakening of the very conducive conditions that have prevailed throughout this Atlantic high-activity era. One key feature of the tropical multidecadal signal seen since 1995 has been an enhanced West African monsoon system (Fig. 4.16b), which is associated with several of the interrelated atmospheric anomalies described previously (Landsea et al. 1998; Bell et al. 1999, 2000, 2004, 2006, 2009; Goldenberg et al. 2001; Bell and Chelliah

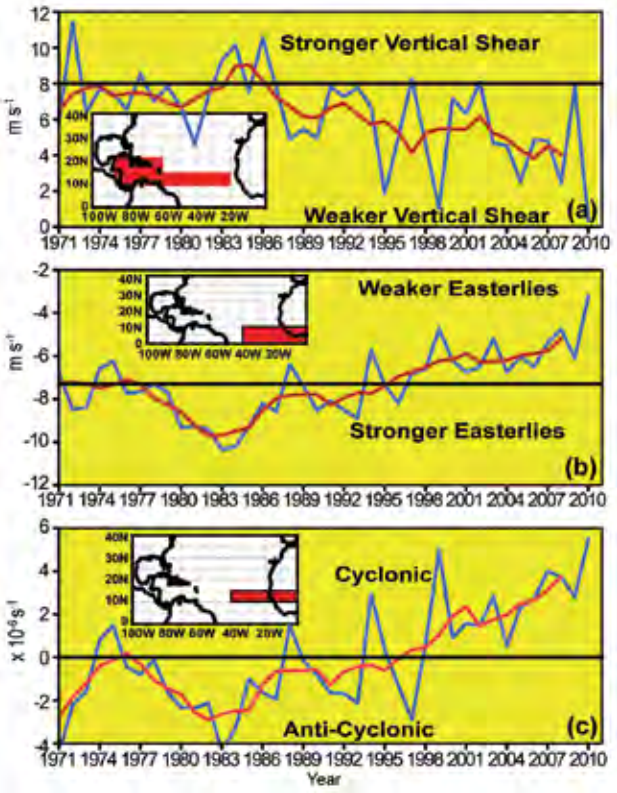

Fig. 4.18. Time series showing consecutive August–October values of area-averaged (a) 200 hPa –850 hPa vertical shear of the zonal wind (m s^{-1}), (b) 700-hPa zonal wind (m s^{-1}), and (c) 700-Pa relative vorticity (x 10^{-6} s^{-1}). Blue curve shows unsmoothed values and red curve shows a five-point running mean of the time series. Averaging regions are shown in the insets.

2006; Kossin and Vimont 2007). These include the enhanced low-level southwesterly flow into the West African monsoon region (Fig. 4.15a) and the enhanced upper-level divergent flow out of that region (Fig. 4.16b). They also include the stronger upper-level ridges over the eastern MDR and across the subtropical South Atlantic (Fig. 4.16a), along with the stronger and westward extended tropical easterly jet.

Accompanying these conditions, the vertical wind shear (Fig. 4.18a) and 700-hPa zonal winds (Fig. 4.18b) remained much weaker in critical parts of the MDR compared to the preceding low-activity era, and the 700-hPa relative vorticity remained cyclonic across the southern MDR rather than anticyclonic (Fig. 4.18c).

Another major climate factor known to affect Atlantic hurricane seasons is ENSO, which produces a combination of vertical shear and atmospheric stability variations (Gray 1984; Tang and Neelin 2004). According to the CPC, La Niña developed during July 2010 (Fig. 4.1), and was a moderate-strength event during August–October.

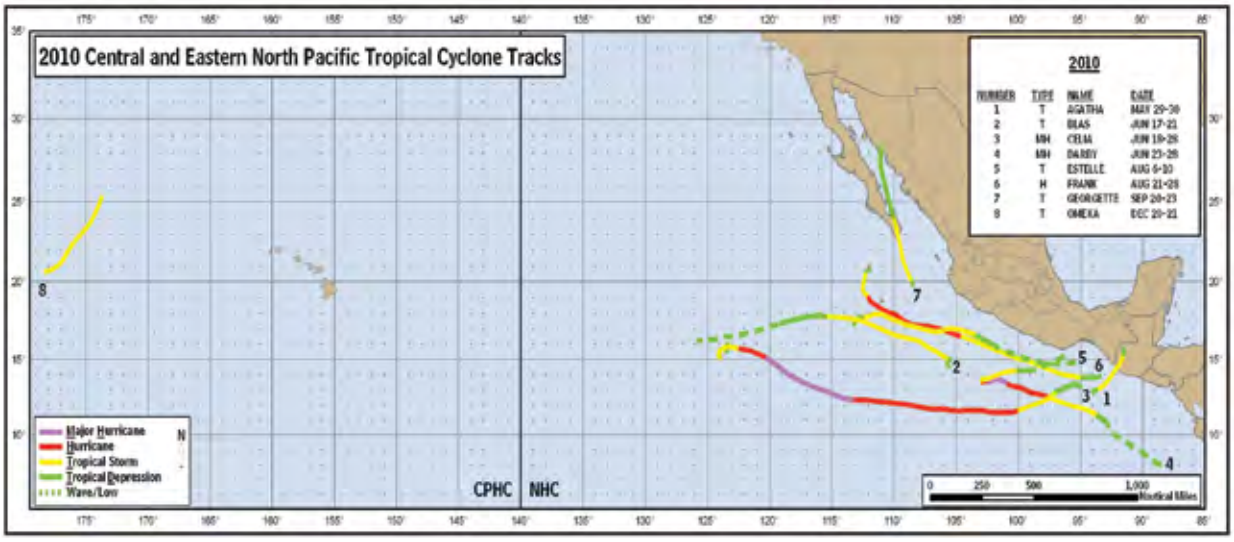

Fig. 4.19. Storm track map for the Eastern Pacific hurricane basins, including all tropical cyclones that occurred in the Eastern North Pacific and Central North Pacific basins [(Source: NOAA's National Hurricane Center (NHC) and Central Pacific Hurricane Center (CPHC)]. Tracks are color coded by intensity (wave/low, tropical depression, tropical storm, hurricane, and major hurricane). Also shown is the delineation of the forecast area of responsibility at 140°W between NOAA's NHC and CPHC.

The 200-hPa velocity potential and divergent wind anomalies across the tropical Pacific Ocean during August–October were consistent with La Niña (Fig. 4.16b), as was the overall zonal wave-1 pattern of 200-hPa streamfunction anomalies in the subtropics of both hemispheres (Fig. 4.16a; Bell and Chelliah 2006). This pattern, which included anticyclonic streamfunction anomalies over the North Atlantic basin and Africa, reinforced that associated with the active Atlantic phase of the tropical multidecadal signal and resulted in the enhanced subtropical ridge extending across the entire MDR. Also within the western MDR, typical La Niña impacts during August–October included the anomalous upper-level easterly winds and decreased vertical wind shear noted previously. These conditions acted to extend westward the anomalously low shear associated with the tropical multidecadal signal.

3) Eastern North Pacific Basin—M. C. Kruk, P. A. Hennon, E. J. Gibney, J. Hobgood, and J. Weyman

(i) Seasonal activity

The Eastern North Pacific (ENP) basin is officially split into two separate regions for the issuance of warnings and advisories by NOAA's National Weather Service (NWS). NOAA's National Hurricane Center (NHC) in Miami, FL, is responsible for issuing warnings in the eastern part of the basin that extends from the Pacific Coast of North America to 140°W, while NOAA's Central Pacific Hurricane Center (CPHC) in Honolulu, HI, is responsible for issuing warnings in the Central North Pacific region between 140°W and the date line. In this section, analysis summarizing the tropical cyclone (TC) activity in both these warning areas is presented using combined statistics, along with information specifically addressing the observed activity and impacts in the central North Pacific (CNP) region.

The ENP hurricane season officially spans from 15 May to 30 November, although storms can develop outside of the official season, especially during El Niño-enhanced hurricane seasons. Hurricane and tropical storm activity in the eastern area of the basin typically peaks in September, while in the Central Pacific, TC activity normally reaches its seasonal peak in August (Blake et al. 2009). Figure 4.19 shows the tracks of all of observed TCs in the ENP and CNP in 2010. For the season as a whole, the number of named storms (NSs), hurricanes, and major hurricanes that developed was less than 50% of the long-term means. Primarily due to the development of La Niña conditions during the boreal summer and early autumn in the equatorial Pacific in 2010, the hurricane season was below average in the ENP basin, with eight NSs, three hurricanes, and two major hurricanes (Fig. 4.20a). These values are far below the 1980–2009 IBTrACS seasonal averages for the basin (21.5 NSs, 12.4 hurricanes, and 6.5 major hurricanes).

Along with the overall below-average activity in 2010 in terms of storm counts, the Accumulated

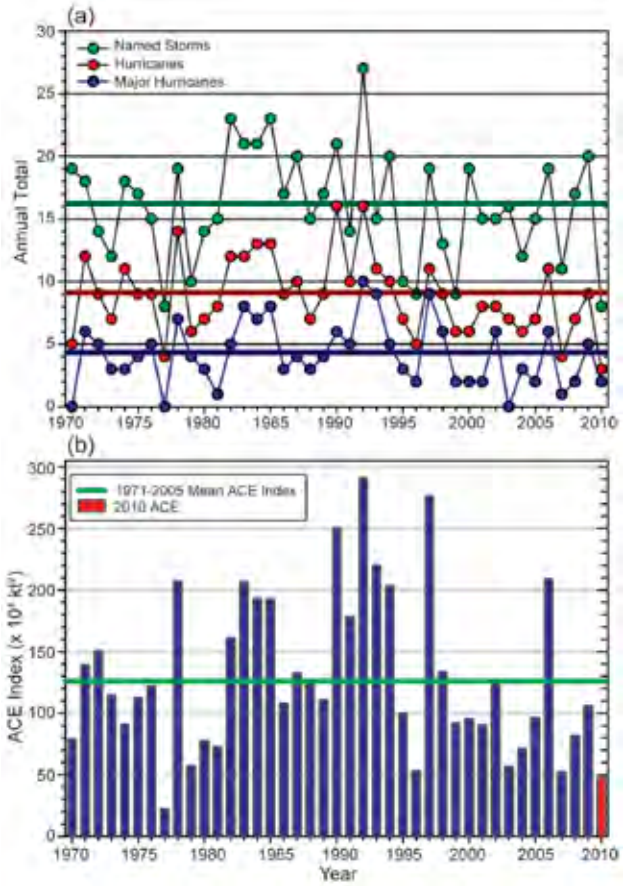

Fig. 4.20. Seasonal tropical cyclone statistics for the Eastern North Pacific (ENP) basin over the period 1970–2010: (a) number of named storms, hurricanes, and major hurricanes and (b) the Accumulated Cyclone Energy (ACE) Index with the seasonal total 2010 highlighted in red. All time series shown include the corresponding 1971–2005 base period means for each parameter.

Cyclone Energy (ACE) Index was also below normal for the basin with a seasonal total of 48.1 × 10^4 kt^2, which is well below the 1971–2005 mean (126.3 × 10^4 kt^2), and is the second lowest ACE season on record since 1975 (Fig. 4.20b).

Just one TC was observed in the CNP region in 2010 (TS Omeka, Fig. 4.19). Tropical Storm Omeka was the latest-forming central and eastern Pacific tropical storm since reliable records began in 1949. On 18 December 2010, the CPHC began monitoring a subtropical cyclone near the date line for possible tropical cyclogenesis. Over the following two days, the system tracked southwestward, entering the western Pacific basin, and began transitioning into a tropical cyclone. Shortly before crossing the date line on 20 December, the CPHC assessed the system to have become a tropical storm. The storm appeared to have reached its maximum intensity west of the date line. The storm was assigned the name Omeka several hours later as it moved into the Central Pacific basin. Shortly after crossing the date line into the central Pacific, wind shear increased, causing the system to weaken. By 21 December, the center of Omeka was devoid of convection and later transitioned into an extratropical cyclone.

Since 1995, the numbers of named storms in the ENP basin has been near average, fluctuating about the long-term mean (Fig. 4.20a). However, the numbers of hurricanes and major hurricanes have been generally below normal in most seasons, with above-normal activity having occurred in only three seasons. NOAA has identified 9 of the 15 seasons in the ENP as being below normal during 1995–2009, with only the El Niño–influenced seasons of 1997 and 2006 producing above-normal activity as measured by the ACE Index (NOAA 2009). In contrast, enhanced activity was observed during the preceding 1970–94 period, which had 6 of 25 (24%) below-normal seasons and 9 of 25 (36%) above-normal seasons, as measured by the ACE Index.

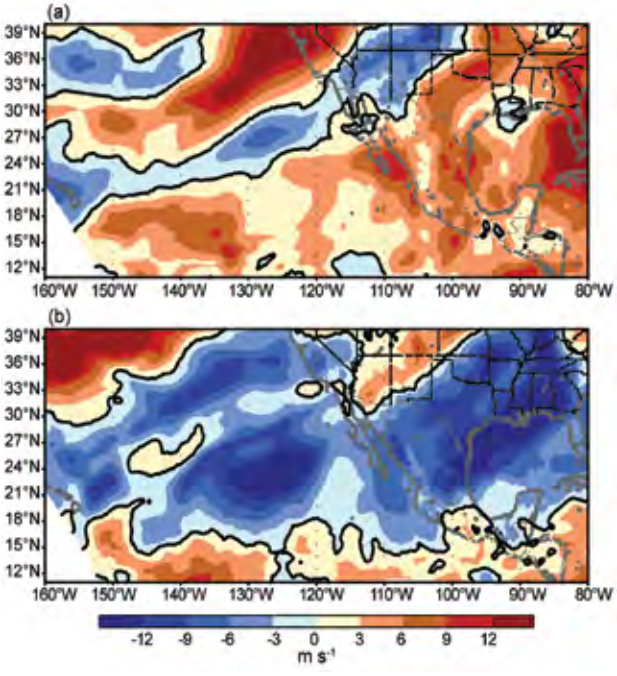

Fig. 4.21. The 200 hPa–850 hPa vertical wind shear anomalies (m s^{-1}) averaged over (a) June–August 2010 and (b) September–November 2010, with anomalies determined relative to the 1979–2004 base period mean. [Source: North American Regional Reanalysis (NARR) dataset, provided by the NOAA National Operational Model Archive and Distribution System.]

(ii) Environmental influences on the 2010 Season

The SSTs in the ENP exhibited a La Niña pattern that intensified as the hurricane season progressed. The cooler-than-normal SSTs extended over much of the ENP where TCs normally develop. The reduction of energy available in the upper ocean contributed to the decreased activity. There was a region of above-normal SSTs early in the hurricane season between latitudes 10°N–20°N and longitudes 120°W–132°W. However, fewer than 9% of ENP TCs normally form over this region and none formed there in 2010. Whitney and Hobgood (1997) suggested that changes of the SSTs in the ENP may be accompanied by a shift in the atmospheric flow pattern over the basin. This appears to have occurred in 2010.

At 850 hPa, the subtropical high was shifted approximately 10° of longitude west of its normal location during the ENP season. This also resulted in above-average vertical wind shear in the 200 hPa–850 hPa layer (Fig. 4.21a). In addition, a stronger-than-normal monsoonal trough extended west and south of Baja California at 850 hPa. The effect of that pattern was to produce anomalous westerly flow over the portion of the ENP where TCs typically form. By itself, the westerly flow might have been favorable for the development of TCs because it would have enhanced the production of low-level vorticity to the north of that flow. However, a stronger-than-normal subtropical ridge at 200 hPa produced faster-than-normal easterly flow over the ENP in the upper levels. The 200-hPa ridge was centered near its usual position in July, but was stronger than normal. By August, the 200-hPa ridge had shifted 15° of longitude east of its normal location. The result of the stronger ridge and eastward shift in its location was to increase the easterly flow over the ENP by 5 m s^{-1} – 10 m s^{-1} during August. However, from September through November, the 200 hPa–850 hPa vertical wind shear across the eastern Pacific basin was anomalously low, by as much as 12 m s^{-1} (Fig. 4.21b). The combination of highly variable wind shear pattern and below-normal SSTs was a potential cause for the quiet 2010 ENP hurricane season. The Quasi-Biennial Oscillation (QBO) phase would have favored more activity (Whitney and Hobgood 1997), but it does not appear to have had a significant impact over the ENP in 2010, consistent with Camargo and Sobel (2010). The fact that Hurricane Celia was able to intensify to a Category 5 level illustrates that, even during less-than-ideal conditions, if a tropical cyclone moves into a favorable environment for a couple of days, it can intensify into a major hurricane.

(iii) Tropical Cyclone Impacts

Just two tropical cyclones made landfall along the Pacific Coast of Mexico during the season (TS Agatha and TS Georgette). In comparison with climatology, the 2010 season is near the 1951–2000 average of 1.34 landfalling TCs (Jauregui 2003).

Along the Pacific Coast of Mexico, TS Agatha (29–30 May) made landfall near the Guatemala-Mexico border, causing widespread flooding. In Guatemala, over 360 mm of rain had fallen by evening on 29 May and resulted in the development of a large sinkhole. Preliminary damage reports suggested that Agatha was responsible for over 300 fatalities in Central America.

On 21 September, short-lived TS Georgette struck the Baja California Peninsula after spending less than a day over open waters. As the cyclone spent so little time over water, its intensity was weak and impacts were virtually negligible. An estimated 66 mm of rain fell in Guaymas and no damage was reported.

The strongest storm of the season in the ENP was Hurricane Celia, which attained Category 5 strength on 25 June with wind speeds of 140 kts (72 m s^{-1}). Two days later, on 27 June, the storm had weakened to tropical storm strength over the open waters of the eastern Pacific. The hurricane appeared impressively annular and had a path from near 98°W to 125°W between 10°N and 15°N. As the storm was so far out to sea, the only impacts were high seas and dangerous rip currents along western Mexico.

4) Western North Pacific basin—S. J. Camargo

The 2010 season featured a total of 19 storms (including five tropical depressions, TDs), forming in the western North Pacific (WNP) basin. Of these 19 active storms in the WNP, 14 reached NS intensity (one was unnamed: TS 2W), eight became typhoons (TYs), and one reached super-typhoon (STY) intensity (Megi). In Fig. 4.22a, the number of TSs, TYs, and STYs per year is shown for the period 1945–2010. The TC data presented here is from the Joint Typhoon Warning Center (JTWC) best-track dataset for 1945–2009 and from preliminary operational data for 2010, for the TCs forming in the WNP basin[6].

[6] It should be noted that there were differences between the 2010 warnings by JTWC and the Regional Specialized Meteorological Center at the JMA in Tokyo—the center responsible for naming the TCs. According to the Japan Meteorological Agency (JMA), 10 additional TDs occurred in 2010. Furthermore, TD 01C, which formed in the Central North Pacific, crossed into the western North Pacific as a tropical cyclone according to the CPHC, be-

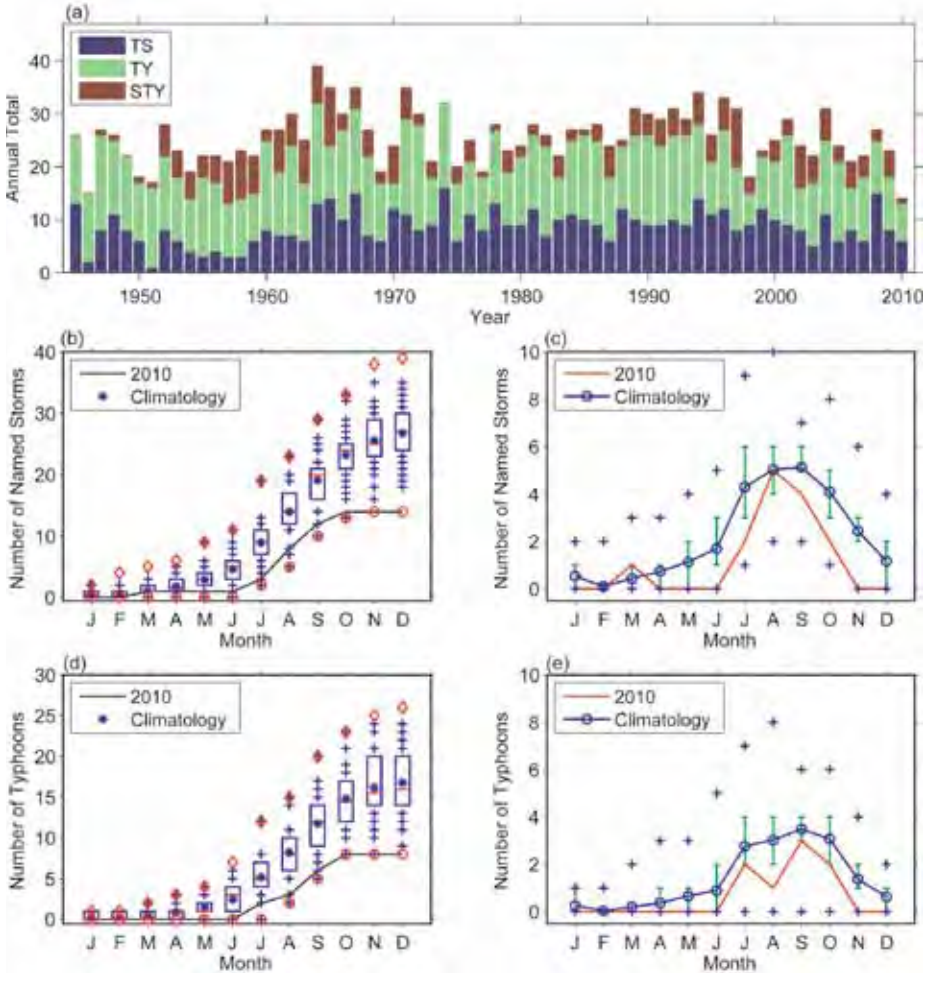

Fig. 4.22 (a) Number of tropical storms (TSs), typhoons (TYs), and super typhoons (STYs) per year in the Western North Pacific (WNP) for the period 1945–2010. (b) Cumulative number of tropical storms with TS intensity or higher (named storms) per month in the WNP: 2010 (black line), and climatology (1971–2000) shown as box plots [interquartile range: box, median: red line, mean: blue asterisk, values in the top or bottom quartile: blue crosses, high (low) records in the 1945–2009 period: red diamonds (circles)]. (c) Number of named storms per month in 2010 (red line), mean climatological number of named storms per month (blue line), the blue plus signs denote the maximum and minimum monthly historical values (1945–2010) and green error bars show the climatological interquartile range for each month. In the case of no error bars, the upper and/or lower percentiles coincide with the median. (d) Cumulative number of typhoons per month in the WNP: 2010 (black line), and climatology (1971–2000) shown as box plots. (e) Number of typhoons per month in 2010 (black line), mean climatological number of TYs per month (blue line), the blue "+" signs denote the maximum and minimum monthly historical values (1945–2010) and green error bars show the climatological interquartile range for each month. [Source: 1945–2009 Joint Typhoon Warning Center (JWTC) best-track dataset, 2010 JTWC preliminary operational track data.]

Climatology is defined using the period 1971–2000; and in addition, this season's activity is far below the 1980–2009 IBTrACS seasonal averages for the basin (26.3 NSs, 15.9 TYs, and 8.0 STYs).

The 2010 WNP TC season started in late January with TD 01W. The first named storm, TS Omais, formed in mid-March (see Fig. 4.22b,c). The WNP was then quiet until July, when TYs Conson and Chanthu occurred. The most active month in terms of number of TCs was August, when five NSs formed in the WNP, though only one reached TY intensity (Kompasu). In September, there were four NSs, three reaching TY intensity (Meranti, Fanapi, and Malakas). Although only two NSs—Megi and Chaba—occurred in October, they were both very intense typhoons, with TY Chaba reaching Category 4. Megi was the only super typhoon in 2010 and ranked among the top 10 strongest typhoons in the historical record for that region. The season finished with TDs 18W and 19W, which formed in November and December, respectively.

The total number of TCs (19), NSs (14), TYs (8), and STYs (1) were all equal or below the bottom fifth percentile of the climatological distributions (median: 30.5 TCs, 27 NSs, 16 TYs, 3 STYs; fifth percentile: 23 TCs, 19 NSs, 11 TYs, 1 STY). Only four previous seasons in the historical record had fewer or the same number of TCs as in 2010, namely 1946 (15 TCs), 1951 (17 TCs), 1950 (18 TCs), and 1954 (19 TCs).

fore crossing the date line again into the Central Pacific. A tropical storm (Domeng) was reported by the Philippine Atmospheric, Geophysical and Astronomical Services Administration in August, and not by JMA or JTWC.

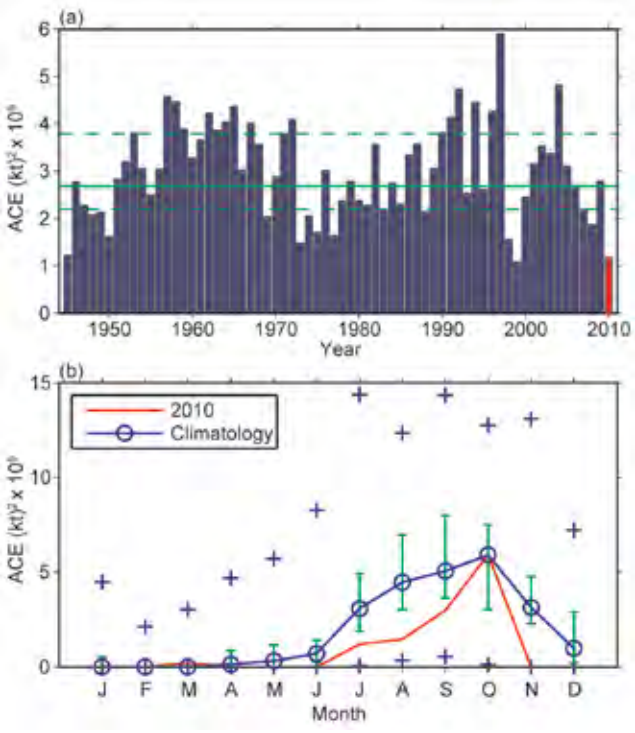

Fig. 4.23 (a) Accumulated Cyclone Energy (ACE) Index per year in the Western North Pacific (WNP) for 1945–2010. The solid green line indicates the median for the climatology years 1971–2000, and the dashed green lines show the climatological 25th and 75th percentiles. (b) ACE Index per month in 2010 (red line) and the median during 1971–2000 (blue line), where the green error bars indicate the 25th and 75th percentiles. In the case of no error bars, the upper and/or lower percentiles coincide with the median. The blue "+" signs denote the maximum and minimum values during the period 1945–2010. [Source: 1945–2009 Joint Typhoon Warning Center (JWTC) best-track dataset, 2010 JTWC preliminary operational track data.]

Note that all these seasons are in the pre-satellite era; therefore, weak storms could have been easily missed in those years. The 2010 season experienced the fewest number of TCs in the WNP in the satellite era. The season also had the lowest number of NSs and TYs in the historical record; the previous records were 15 NSs (in 1946) and nine TYs (in 1998). As the Eastern North Pacific hurricane season was very quiet as well in 2010, the entire North Pacific had a very low level of tropical cyclone activity in 2010. The cumulative distribution of NSs (Fig. 4.22b) and TYs (Fig. 4.22c) shows a very slow season start, with activity increasing in July and August, and flattening after October, never reaching the climatological cumulative values in the region. The only months in which the NSs reach the climatological medians are March and August. However, only one of the August NSs intensified to a TY, an uncommon occurrence in the region (August 1946: no TYs; August 1976, 1977, 2006, and 2008: one TY).

The accumulated cyclone energy (ACE) in the WNP (Fig. 4.23) reflects well the activity in NSs. The 2010 season ACE was the second lowest such value in the historical record. Only in 1999 did a lower value of ACE occur in the region. The monthly ACE values were in the bottom quartile of the climatological distribution in the peak months of the season (June–November), with the exception of October, when the ACE value reached the climatological median for that month. Super Typhoon Megi was responsible for this higher ACE value in October, corresponding to 71% of the ACE for that month and 36% of the ACE for the 2010 season. The ACE value of STY Megi was in the top one percentile of the historical and climatological distributions of ACE per storm.

There were only 74 days with TCs and 64 days with NSs in 2010 in the WNP, both record low values in the historical record (climatological medians: 161.5 and 144.25 days, respectively). From these active days, only 52.5 days had TYs, another record of lowest value in the historical record (climatological median 120.4 days). There were 8.25 days with intense TYs (Categories 3–5), the seventh lowest in the historical record (25th climatological percentile is 11 days). Climatologically, 74% (11%) of the TC days consist of days with (intense) TYs, very close to the rates in 2010—71% (11%). The median lifetime of NSs in 2010 was 5.5 days, below the climatological 25th percentile lifetime of 5.75 days. From the 14 NSs, 12 had a lifetime below the climatological median (eight days), and seven were in the bottom quartile of the climatological distribution. Only STY Megi had a lifetime (11.5 days) in the top quartile of the distribution (above 11.25 days).

The mean genesis location (17.1°N, 130.9°E) in 2010 was shifted northwest of the climatological mean genesis positions (12.9°N, 143.5°E). The mean track position (22.0°N, 125.0°E) was also shifted slightly northwestward of the climatological mean (19.0°N, 134.2°E). These shifts are consistent with typical La Niña events, which tend to have a northwestward genesis shift (Chan 1985; Chia and Ropelewski 2002). Many of the characteristics of the 2010 TY season are typical of La Niña events, such as: a northwestward track shift, few intense storms, low ACE values, and short-lived storms. The influence of ENSO events on the characteristics of the WNP tropical cyclone activity are well known (e.g., Wang and Chan 2002; Camargo and Sobel 2005; Camargo et al. 2007a,b).

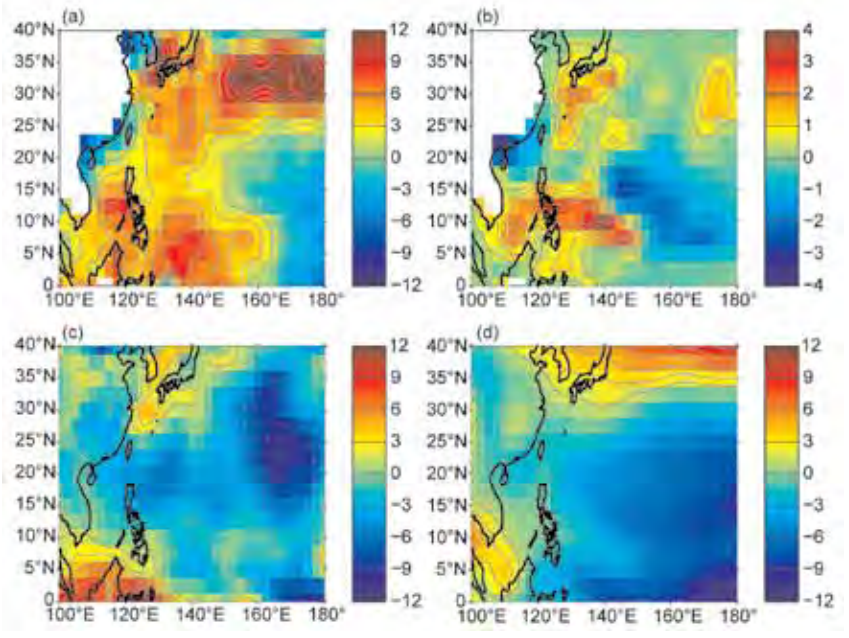

Fig. 4.24. (a) Potential intensity anomalies for July–October (JASO) 2010 from 1971–2000 climatology in m s^{-1}; (b) genesis potential index anomalies for JASO 2010; (c) 600-hPa relative humidity anomalies for JASO 2010 (in %); (d) 850-hPa zonal winds for JASO 2010. Contour interval in (a), (c,) and (d) is 1.5, in (b) contour interval is 1; positive contours are shown in solid lines, negative contours in dash dotted lines and the zero contour line in a dotted line. [Source: atmospheric variables: NCEP Reanalysis data (Kalnay et al. 1996); sea surface temperature (Smith and Reynolds 2005).]

La Niña conditions were present for a good portion of the TY season and were probably responsible for the low activity in the TY season of 2010. Based solely on ENSO SST indices, such as Niño-3.4 (Barnston et al. 1997), this La Niña event would be considered a moderate one. However, the event was quite strong when including the atmospheric component. The Southern Oscillation Index and the multivariate ENSO index (MEI; Wolter and Timlin 1993, 1998) both indicate the 2010 La Niña event as one of the strongest in the historical record. The MEI rank for this event during the TY season was either the strongest (August–September) or the second strongest (July–August and September–October periods); see http://www.esrl.noaa.gov/psd//people/klaus.wolter/MEI/rank.html.

Figure 4.24 shows the environmental conditions responsible for the low level of activity in 2010. The potential intensity (Emanuel 1988, 1995; Fig. 4.24a) shows a large region of negative anomalies near the date line. Similarly, the genesis potential index (GPI; Camargo et al. 2007a) shows negative anomalies in the eastern part of the basin (Fig. 4.24b). The strength and size of these negative anomalies are larger than during most La Niña years. The two years (since 1950) that have most similar patterns for the potential intensity and GPI are 1950 and 1999, which also had very low activity in the WNP. The negative anomalies of the midlevel relative humidity at 600 hPa (Fig. 4.24c) contributed to the negative anomalies in the GPI in the basin. In most La Niña events, there is an increase of GPI near the Asian continent, which is attributed mainly to an increase in relative humidity (Camargo et al. 2007a). In 2010, the region of increased relative humidity was shifted more northward (near Japan) than in other La Niña events. The decreased GPI near the date line in La Niña events is attributed mainly to the low-level vorticity, with some contribution from the vertical shear and midlevel relative humidity (Camargo et al. 2007a). This was also the case in 2010 (not shown). Very strong easterly anomalies in the region throughout the typhoon season led to a monsoon trough with an eastern extent restricted to a small region west of the Philippines (also typical of La Niña years), as shown in Fig. 4.24d, which further contributed to the low activity observed in 2010.

Eleven WNP TCs made landfall during 2010, which is below the 1951–2000 median of 15[7]. Two systems made landfall as a TD (median is three), five made landfall as a TS (median is six), and three struck as a TY (median is four). Megi made landfall as a Category 5 STY. Megi was one of the most intense landfalling tropical cyclones in the historical record, not only in the WNP, but globally.

As could be expected, the largest impacts in this TY season were due to STY Megi. The storm made landfall in the mountain range of Sierra Madre, Luzon Island, in the Philippines. According to a United Nations report (OCHA 2010), almost two million people were affected by the typhoon, mainly

[7] Here we consider only one landfall per TC. If a TC makes more than one landfall, the landfall event with the highest wind speed is considered.

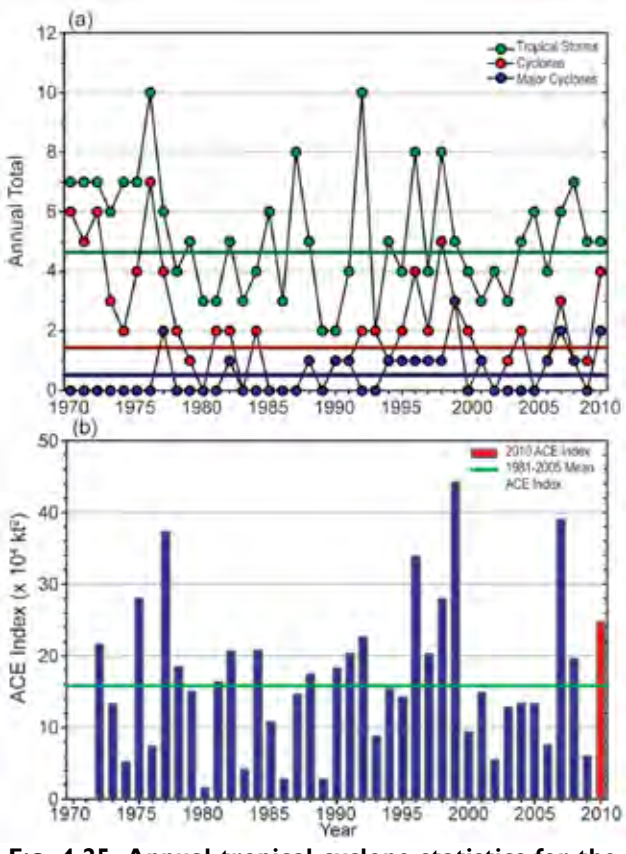

Fig. 4.25. Annual tropical cyclone statistics for the North Indian Ocean (NIO) over the period 1970–2010: (a) number of tropical storms, cyclones and major cyclones and (b) the estimated annual Accumulated Cyclone Energy (ACE) Index (in $kt^2 \times 10^4$) for all tropical cyclones during which they were at least tropical storm strength or greater (Bell et al. 2000). The 1981–2005 base period means are included in both (a) and (b). Note that the ACE Index is estimated due to a lack of consistent six-hour sustained winds for every storm.

in Isabella province. There were 19 deaths associated with the storm. Approximately 30 200 houses were destroyed, and 116 000 were partially damaged. There was an estimated 80% loss of crops, such as rice and corn in the Province of Isabella, which is the second largest producer of rice in the Philippines.

Typhoon Mindulle also had a large impact. The storm brought heavy rainfall to Vietnam, leading to significant flooding and agricultural losses in that country, as well as the death of many fishermen.

5) Indian Ocean Basins

(i) North Indian Ocean—M. C. Kruk and K. L. Gleason

The North Indian Ocean (NIO) TC season typically extends from April to December, with two peaks in activity during May–June and November when the monsoon trough is positioned over tropical waters in the basin. Tropical cyclones in the NIO basin normally develop over the Arabian Sea and Bay of Bengal between latitudes 8°N and 15°N. These systems are usually short lived and relatively weak, and often quickly move into the Indian subcontinent. However, strong and "severe cyclonic storms" (Holland 1993) can develop with winds exceeding 130 kts (67 m s^{-1}; Neumann et al. 1993).

The 2010 TC season produced five named storms (NSs), four cyclones (CYC), and two major cyclones (MCYC; Fig. 4.25a). These values, except for NSs, are above the 1980–2009 IBTrACS seasonal averages of 6.3 NSs, 1.7 CYCs, and 0.8 MCYCs. The season produced an ACE Index value of 24.7 x 10^4 kt^2, which is above the 1981–2005 mean of 16 x 10^4 kt^2 (Fig. 4.25b). There is generally an enhancement in TC activity, especially in the Bay of Bengal, during La Niña (Singh et al. 2000), which the globe was transitioning to during the boreal summer 2010.

The first CYC of the season developed in the Bay of Bengal from 17 to 21 May and became CYC Laila with maximum sustained winds of 65 kts (33 m s^{-1}). Laila underwent rapid intensification before making landfall near Bapatla, Andhra Pradesh, on 20 May. Damage was extensive in Andhra Pradesh and more than a dozen persons were killed by the storm. Parts of the region experienced 24-hour rainfall totals between 320 mm and 510 mm.

The two MCYCs of the season occurred 31 May–6 June (Phet) and 21–22 October (Giri). Major Cyclone Phet developed in the Arabian Sea and eventually made landfall in Oman [125 kts (64 m s^{-1})] where first estimates of damages exceeded $780 million (U.S. dollars; http://in.reuters.com/article/2010/06/07/idINIndia-49106920100607). Phet was the second strongest storm on record to develop in the Arabian Sea (behind only MCYC Gonu in 2007). Major Cyclone Giri developed in the Bay of Bengal and made landfall near Kyaukpyu, Myanmar, with maximum sustained winds of 135 kts (69 m s^{-1}). The cyclone intensified into a Category 5 storm in just over a 24-hour period. Tens of thousands of citizens were displaced by the approximate 3.7-m storm surge and heavy rains that accompanied MCYC Giri. Over 150 people were believed to be killed by the storm.

The 2010 season ended with CYC Jal, which had maximum sustained winds of 70 kts (36 m s^{-1}). The track of CYC Jal was nearly identical to that of CYC Laila. Jal occurred 4–7 November and began as a weak disturbance in the South China Sea. The storm

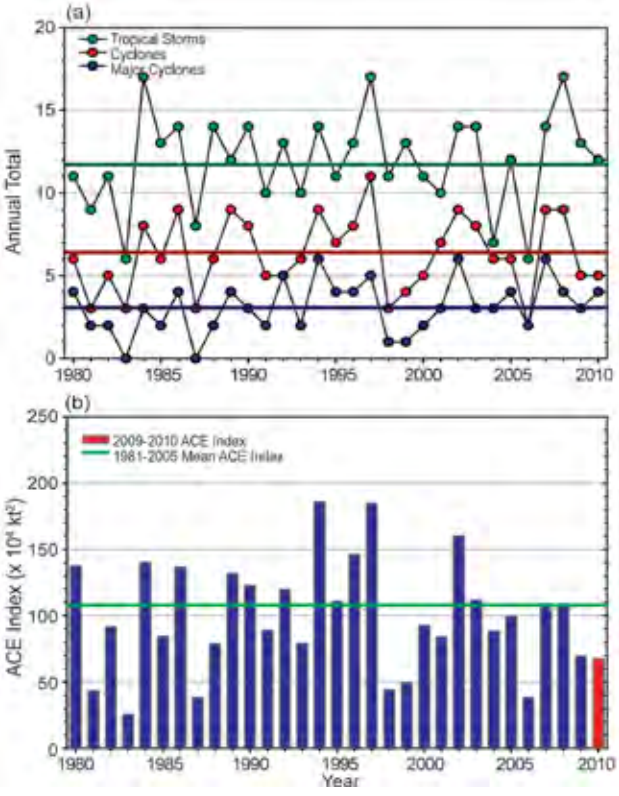

Fig. 4.26. Annual tropical cylone statistics for the Southern Indian Ocean (SIO) over the period of 1980–2010: (a) number of tropical storms, cyclones and major cyclones and (b) the estimated annual Accumulated Cyclone Energy (ACE) Index (in $kt^2 \times 10^4$) for all tropical cyclones during which they were at least tropical storm strength or greater (Bell et al. 2000). The 1981–2005 base period means are included in both (a) and (b). Note that the ACE Index is estimated due to a lack of consistent six-hour sustained winds for every storm.

intensified to Category 1 strength before weakening as it headed toward the Indian coast. Jal produced widespread flooding and mudslides, and devastated the local rice crop. The storm was blamed for 54 fatalities in Andhra Pradesh.

(ii) South Indian Ocean—K. L. Gleason and M. C. Kruk

The South Indian Ocean (SIO) basin extends south of the Equator from 105°E to the African coastline[8], with most CYCs developing south of 10°S. The SIO TC season extends from July to June encompassing equal portions of two calendar years (i.e., the 2010 season is comprised of storms from July to December 2009 and January to June 2010). The peak activity typically occurs from December to April when the ITCZ is located in the Southern Hemisphere. Historically, the vast majority of landfalling CYCs in the SIO impact Madagascar, Mozambique, and the Mascarene Islands, including Mauritius and Réunion.

The historical SIO TC data is probably the least reliable of all the TC basins (Atkinson 1971; Neumann et al. 1993), primarily due to a lack of historical record keeping by individual countries and no centralized monitoring agency; however, the historical dataset for the region has been updated (Knapp et al. 2010). The historical data are noticeably deficient before reliable satellite data were operationally implemented in the region beginning about 1983.

The 2009/10 SIO season storm numbers were below average with 12 NSs, 5 CYCs, and 4 MCYCs (Fig. 4.26a). The 1980–2009 IBTrACS seasonal averages are 17.5 NSs, 8.9 CYCs, and 4.6 MCYCs. In addition, the 2009/10 ACE Index (~68 x 10^4 kt^2) was below the 1981–2005 average (Fig. 4.26b). With the exception of the 2001/02 season, each season since the mid-1990s has produced a near-average or below-average seasonal ACE in the SIO basin.

The strongest storm during the season was MCYC Edzani, which developed in the central Indian Ocean, north of the Cocos Islands during the first few days of January 2010. The disturbance initially showed two low-level circulation centers before they merged. As it became more organized, the system was upgraded to a tropical depression and continued to intensify over the next several days. Edzani became a strong Category 4 MCYC on 8 January with maximum sustained winds of 135 kts (69 m s^{-1}). At peak intensity, Edzani was located approximately 590 n mi east-southeast of Diego Garcia and continued on a west-southwestward track into cooler waters and an environment with stronger wind shear. By 14 January, Edzani had substantially weakened and was classified as extratropical by the Joint Typhoon Warning Center. Edzani remained over open ocean waters during its lifecycle and had little to no impact on land.

Only two TCs made landfall in the basin during the season. Tropical Storm Fami developed on 2 February in the Mozambique Channel and came ashore on the west side of Madagascar near Belo sur Mer with maximum sustained winds of 40 kts (21 m s^{-1}). While over land, Fami developed an eye-like feature in the mid-to-upper levels of the cyclone, which indicated it was maintaining strength. Friction from the land and wind shear caused Fami to dissipate prior to reemerging over open waters. Tropical Storm Hubert formed in the ocean waters east of Madagascar on 10 March

[8] In order to generate consistent basin statistics, the SIO basin boundary overlaps with the Australian Bureau of Meteorology's operational warning area from 90°E to 105°E.

and made landfall near Mahaela with sustained winds of 35 kts (18 m s^{-1}). Bringing heavy winds and rain to the already saturated soil in southeast and south-central Madagascar, TS Hubert began to dissipate and became a heavy rain event once on land. Most of the strongest winds and heaviest rains stayed south and east of the capital city of Antananarivo, although landslides and flooding stranded people in many towns and villages, disrupted communications and electricity, and caused at least 70 deaths.

6) Southwest Pacific Basin—A. M. Lorrey, S. McGree, J. Renwick, and S. Hugony

During the 2009/10 TC season, New Zealand's National Institute of Water and Atmosphere (NIWA) forecast normal activity for most island nations and territories in the southwest Pacific region (between 135°E and 120°W). The overall TC activity was expected to be near normal, with 8–11 storms forecast for the 2009/10 season. Two or three storms were forecast to reach at least Category 3[9], and one storm was expected to reach at least Category 4, with mean wind speeds of at least 64 kts (33 m s^{-1}). Documentation of the TC activity during the season was collated from reports issued by the Regional Specialized Meteorological Center in Nadi, Fiji, the Australia Bureau of Meteorology, the Tropical Cyclone Warning Centre based at the New Zealand Meteorological Service in Wellington, and the Joint Typhoon Warning Center (JTWC).

In the Southwest Pacific sector, a total of ten TCs were documented for the season. The onset of the season did not occur until early December 2009. The storms that occurred during the first two months of the season (Mick, Neville, Olga, and Nisha) achieved only a Category 1 or 2 status. In contrast, the second half of the season from February to April saw the development of five systems that reached or exceeded Category 3 status (Oli, Pat, Rene, Tomas, and Ului). Three Category 4 storms had winds in excess of 86 kts (44 m s^{-1}; Oli, Rene, and Tomas), and one event had 10-minute sustained winds in excess of 108 kts (56 m s^{-1}; Ului). Tropical Cyclone Sarah, which formed on 26 February, 270 n mi northwest of Rarotonga in the Cook Islands, only attained Category 1 status.

The existence of El Niño saw the tropical and subtropical limbs of the South Pacific Convergence Zone (SPCZ) located to the northeast of their climatological positions during the season. This helped guide a number of tracks to the east of the date line, with ex-tropical transitions oriented to the southeast for some storms. The regional ENSO conditions and influence of the SPCZ's geometry were especially obvious for the second half of the TC season, which saw elevated TC activity in French Polynesia and the Southern Cook Islands (SCI). Of note, a traditional environmental knowledge climate indicator used in the SCI and elsewhere in the southwest Pacific (timing of mango flowering) was highlighted prior to the onset of the season by the director of the Cook Islands Meteorological Service. Based on the early flowering of the mangoes, it was suggested the TC season would see increased risk to the east of the date line. This piece of indigenous climate guidance compared favorably with the TC guidance issued by NIWA in October 2009, and the forecasted conditions came to fruition beginning in January 2010[10]. It should also be noted that the analog climate guidance[11] generated from looking at past seasonal activity was provided in the February 2010 update and suggested an increased risk in the Solomon Islands/north Coral Sea region. While this was apparently an odd component of the projection for an El Niño year, the new guidance was timely, and provided a three-week lead time prior to the onset of TC Ului (Category 5) that passed south of the Solomon Islands.

The onset of significant TC activity to the east of the date line was first observed for TC Oli, which impacted French Polynesia. This storm produced strong swells and made a direct impact on the island of Tubuai (Austral Islands). Oli crossed more than 2700 n mi from 1 to 6 February while in transit through the Southwest Pacific Ocean. It reached Category 2 status while passing by Mopelia Island, and the track then veered to the southwest of the Windward Islands before closing on Tahiti and Moorea late on 3 February. There were 39 kt (20 m s^{-1}) maximal 10-minute sustained winds, with gusts of 57 kts (29 m s^{-1}) recorded at Bora-Bora, and very high seas were noted with waves estimated at 6.1 m across the Society Island group.

[9] Storm categorizations in this basin are based on the Australian TC scale and not Saffir-Simpson See http://www.bom.gov.au/weather/cyclone/faq/index.shtml for a definition of Australian TC categories.

[10] The scientific community is beginning to pay more attention to the value of traditional environmental knowledge and this information is included here in that light. See King et al. (2008) and Lefale (2010) as examples of the work being done in this area of research in the Pacific.

[11] See <http://www.niwa.co.nz/our-science/pacific-rim/news/featured/tropical-cyclone-outlook-normal2/background-information-for-meteorological-services> regarding the analog methodology employed here.

Several houses as well as some hotels were destroyed or partly damaged by strong winds and waves from TC Oli, but fortunately on Tahiti and Moorea there was only minimal damage, with some roofs torn off and coastal detritus washed up on the shore due to the significant wave activity. Oli intensified after passing Tahiti, reaching Category 4 status, and inflicted damage on Rurutu and Raivavae from wind and waves with estimated heights of 8 m. Only a few hours after the arrival of TC Oli on Tubuai, there was significant wave damage up to 100 m inland. The eye of TC Oli passed over Tubuai on 5 February, with a minimum sea level pressure of 955.8 hPa recorded and sustained winds of 55 kts (28 m s^{-1}), with gusts up to 92 kts (47 m s^{-1}). The northern and northeastern coasts of Tubuai were devastated, in contrast with southern, sheltered coastal areas.

The breadth of latitude covered by the Cook Islands meant that this island nation was battered by several tropical cyclones during the 2009/10 season. After feeling the effects of TC Oli, TC Pat (Category 3) directly impacted Aitutaki, Southern Cook Islands. Strong winds blowing consistently at 100 kts (51 m s^{-1}), with gusts up to 130 kts (67 m s^{-1}), for up to four hours overnight ripped off roofing, uprooted coconut palms and trees, damaged water tanks, and destroyed the local electricity distribution network by taking down power poles and lines. Many people took shelter on high ground in a local church, and the damage was significant enough for the Prime Minister to declare a state of disaster. It was suggested by eyewitnesses who are elders in the Aitutaki community that this was the worst storm to affect the island in living memory. These observations are very much in-line with emerging research related to traditional environmental knowledge that contributes to increased awareness of weather and climate risks in the region (King et al. 2008; Lefale 2010). For example, the ability and knowledge of the Samoans to forecast the onset of extreme weather and climate events, relying predominantly on local environmental changes, are vital tools that can be incorporated in the formulation of climate change adaptation strategies and contemporary weather forecasts (Lefale 2010).

Severe TC Rene (Category 4) affected American Samoa and Tonga in mid-February, with significant damage to roads and agricultural infrastructure from heavy rainfall in Samoa. Damage to buildings, electricity infrastructure, and roads were reported for Tonga, which experienced a direct impact from the storm eye. Subsequently, TC Sarah (Category 1) affected the Northern Cook Islands, but with no reports of major damage or fatalities. The brief respite from intense TC activity was curtailed with the joint onset of TCs Ului (Category 5) and Tomas (Category 4). The combination of these systems wreaked havoc across the central and northwest corners of the southwest Pacific during the second week in March. Ului caused significant flooding and damage in the Solomon Islands, while Tomas affected the island of Vanua Levu, Fiji, ripping off corrugated roofing iron and forcing thousands to take shelter in evacuation centers. "Overwhelming" damage was reported in the northern and eastern parts of the country by the Prime Minister of Fiji. Sea surges of up to 7 m were reported in the Lau Group in the eastern part of the country.

Overall, the TC activity in the region was in the normal range for the season, as forecast; however, the strength of many systems that developed during the latter part of the season, including three Category 4 storms and one Category 5 storm, were highlighted on the global stage (Terry and Etienne 2010) as the minimum estimated damage for the 2009/10 season was estimated at $163 million (U.S. dollars), and 14 fatalities were reported for the region as a result of seasonal TC activity.

7) Australian Region Basin—B. C. Trewin

(i) Seasonal Activity

The 2009/10 TC season was slightly below normal in the broader Australian basin (areas south of the Equator and between 90°E and 160°E[12], which includes Australian, Papua New Guinea, and Indonesian areas of responsibility). The season produced eight TCs, below the long-term average of 10. There were three TCs in the eastern sector[13] of the Australian region during 2009/10 (one of these entering from the Southwest Pacific region), four TCs in the western sector (one of which formed in the northern sector), and one in the northern sector. There were five landfalls during the season.

[12] The Australian Bureau of Meteorology's warning area overlaps both the southern Indian Ocean and Southwest Pacific.

[13] The western sector covers areas between 90°E and 125°E. The eastern sector covers areas east of the eastern Australian coast to 160°E, as well as the eastern half of the Gulf of Carpentaria. The northern sector covers areas from 125°E east to the western half of the Gulf of Carpentaria.

(ii) Landfalling and Other Significant Tropical Cyclones

The most intense TC of the season was Laurence, which affected Western Australia in mid-December. Laurence reached TC intensity on 14 December 2009 in the Joseph Bonaparte Gulf near 13°S, 128°E (approximately 135 n mi north of Wyndham, Western Australia). By the time it approached the north coast of Western Australia near Troughton Island, it had intensified to Category 3 intensity[14], then further intensified to Category 5 intensity as it moved southwest, parallel to the coast. Its initial intensity peak occurred on 16 December at 15.3°S, 124.2°E (offshore from Kuri Bay), with estimated maximum gusts of 155 kts (79 m s^{-1}), maximum sustained winds of 110 kts (56 m s^{-1}), and a minimum central pressure of 932 hPa. Laurence made landfall as a Category 3 system late on 16 December on a remote section of the coast northeast of Derby. After weakening to a tropical depression as it moved over land, it reintensified to a TC as it moved over water north of Broome on 19 December, and continued to intensify as it moved southwest, ultimately regaining Category 5 intensity on 21 December [maximum gusts 155 kts (79 m s^{-1}), maximum sustained winds 110 kts (56 m s^{-1}), minimum central pressure 929 hPa]. It made landfall shortly thereafter near Wallal, about 135 n mi east of Port Hedland. Both landfalls took place in sparsely populated areas and there was only limited wind damage, but heavy rain caused flooding and stock losses in the region east of Port Hedland. While weakening below TC intensity as it moved southeast, Laurence maintained its identity as a system well into the central continent, ultimately causing flooding as far east as northern New South Wales. Laurence was the first Category 5 landfall on the Australian mainland since George in March 2007; over the last 25 years, Category 5 landfalls have occurred once every three to four years on average.

Ului moved into the Australian region from the Southwest Pacific region on 15 March. Having reached Category 5 intensity [maximum gusts 155 kts (79 m s^{-1}), maximum sustained winds 115 kts (59 m s^{-1}), minimum central pressure 930 hPa] near 13°S, 161°E, just before entering the Australian region, it moved southwest across the Coral Sea while in a slowly weakening phase. It reintensified slightly before crossing the Queensland coast near Airlie Beach as a Category 3 system early on 21 March. Significant wind damage occurred between Airlie Beach and Mackay, with widespread crop and tree damage and power outages, and many boats in coastal harbors were damaged or destroyed by large seas and swell.

The other severe TC of the season was Magda, which made landfall as a Category 3 system near Kuri Bay (a very similar location to the first landfall of Laurence) on 22 January. The landfall region is very sparsely populated and only minor damage was reported. The other two landfalling systems of the season, both of which peaked at Category 2 and made landfall as Category 1 systems, were Olga, which made landfall on the Gulf of Carpentaria coast west of Karumba, Queensland, on 30 January (having earlier reached TC intensity in the Coral Sea and crossed the southern Cape York Peninsula as a tropical depression), and Paul, which made landfall on the Arnhem Land coast of the western Gulf of Carpentaria northwest of Groote Eylandt on 29 March. Both TCs brought heavy rain and subsequent flooding, particularly Paul, which produced 443 mm at Bulman, Northern Territory, on 31 March, the highest daily rainfall total in Australia in 2010.

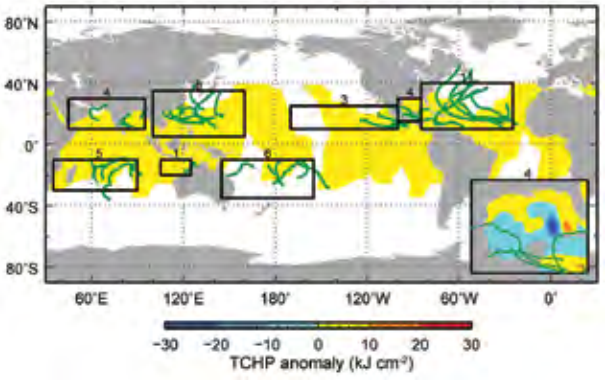

Fig. 4.27. Global anomalies of Tropical Cyclone Heat Potential (TCHP) corresponding to 2010 computed as described in the text. The boxes indicate the seven regions where tropical cyclones occur: from left to right, Southwest Indian, North Indian, West Pacific, Southeast Indian, South Pacific, East Pacific, and North Atlantic (shown as Gulf of Mexico and tropical Atlantic separately). The green lines indicate the trajectories of all tropical cyclones reaching at least Category 1 [one-minute average wind ≥ 64 kts (33 m s^{-1})] and above during November 2009–April 2010 in the Southern Hemisphere and June–November 2010 in the Northern Hemisphere. The numbers above each box correspond to the number of Category 1 and above cyclones that travel within each box. The Gulf of Mexico conditions during June–November 2010 are shown in detail in the insert shown in the lower right corner.

[14] Storm categorizations in this basin are based on the Australian TC scale and not Saffir-Simpson. See http://www.bom.gov.au/weather/cyclone/faq/index.shtml for a definition of Australian TC categories.

Three other TCs failed to make landfall: Neville (Category 1) in the Coral Sea in January, and Robyn and Sean (both Category 2) in the Indian Ocean in April. None had any impact on land areas.

e. *Tropical Cyclone Heat Potential*—G. J. Goni, J. A. Knaff, and I-I Lin

Variations in the Tropical Cyclone Heat Potential (TCHP) in each of the seven tropical cyclone basins are discussed in this section. The TCHP is defined as the ocean heat content contained between the sea surface and the depth of the 26°C isotherm. It has been shown that high TCHP values are more closely linked to intensity changes than SST (Shay et al. 2000; Goni and Trinanes 2003; Lin et al. 2008, 2009), provided that atmospheric conditions are also favorable.

Although SST data provide a measure of the surface ocean conditions, the data give no information about the subsurface (first tens of meters) ocean thermal structure. It is known that the ocean skin temperature erodes when the sea surface is affected by strong winds, creating a well-mixed layer that can reach depths of several tens of meters. As the TC progresses, it travels above waters with mixed layer temperatures similar to their skin temperatures. This provides the motivation to investigate and monitor the upper ocean thermal structure, which has become a key element in the study of tropical cyclone intensifications focused on predictions of sudden TC intensification. In addition, the inclusion of TCHP in statistical models has been shown to reduce intensity prediction errors for the most intense cyclones. Research has shown how the upper ocean thermal structure is a good indicator for predicting TC intensity (Mainelli et al. 2008).

Fields of TCHP show high spatial and temporal variability associated with oceanic mesoscale features that can be detected globally using satellite altimetry (Lin et al. 2008; Goni et al. 2009). It has been shown that areas with high values of TCHP can be an important factor for TC intensification (e.g., Shay et al. 2000; Mainelli et al. 2008). To examine the interannual variability of TCHP with respect to tropical cyclones, TCHP anomalies are computed during the months of TC activity in each hemisphere: June–November in the Northern Hemisphere and November–April in the Southern Hemisphere. Anomalies are defined as departures from the mean TCHP calculated during the same months for the period 1993–2010. These anomalies show large variability within and among the tropical cyclone basins (Fig. 4.27).

The west Pacific basin generally exhibits the anomalies related to ENSO events, with 2010 being characterized by the onset of La Niña conditions, which have been in place in the equatorial Pacific Ocean since approximately June 2010. Similar to the conditions during 2008 and 2009, the South Pacific basin showed mostly positive anomalies. The north Indian basin exhibited positive values in the Bay of Bengal and in the Arabian Sea. The Gulf of Mexico (Fig. 4.27 insert, lower right) showed mostly negative values except for a region of positive values in the northern region. Similar to 2009, the tropical Atlantic exhibited mostly positive values, which is also observed in sea height and SST fields (http://www.aoml.noaa.gov/phod/regsatprod/atln/index.php). The most evident changes in TCHP between 2010 and 2009 are the decrease in values in the Gulf of Mexico and the southwestern Pacific Ocean and the increase in values in the western Pacific Ocean, Arabian Sea, and Bay of Bengal (Fig. 4.28).

During 2010, a number of major TCs were positively identified to have gained strength when traveling into regions of high values of TCHP, three TCs exhibited a weak link, and three did not show any link between ocean heat content and intensification. Some examples of these intensification events are shown in Fig. 4.29. The results presented here correspond to four major TCs, where the location of their intensification coincided with an increase of the values of TCHP along their tracks. These TCs were Igor (tropical Atlantic), Celia (Eastern North Pacific, ENP), Megi (Western North Pacific, WNP), and Phet (Arabian Sea). The cooling associated with the wake of intense TCs, which reached

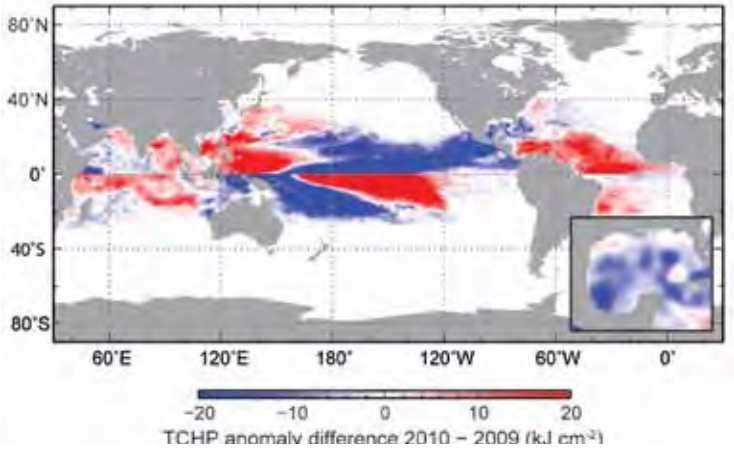

Fig. 4.28. Differences between the Tropical Cyclone Heat Potential (TCHP) fields in 2010 and 2009.

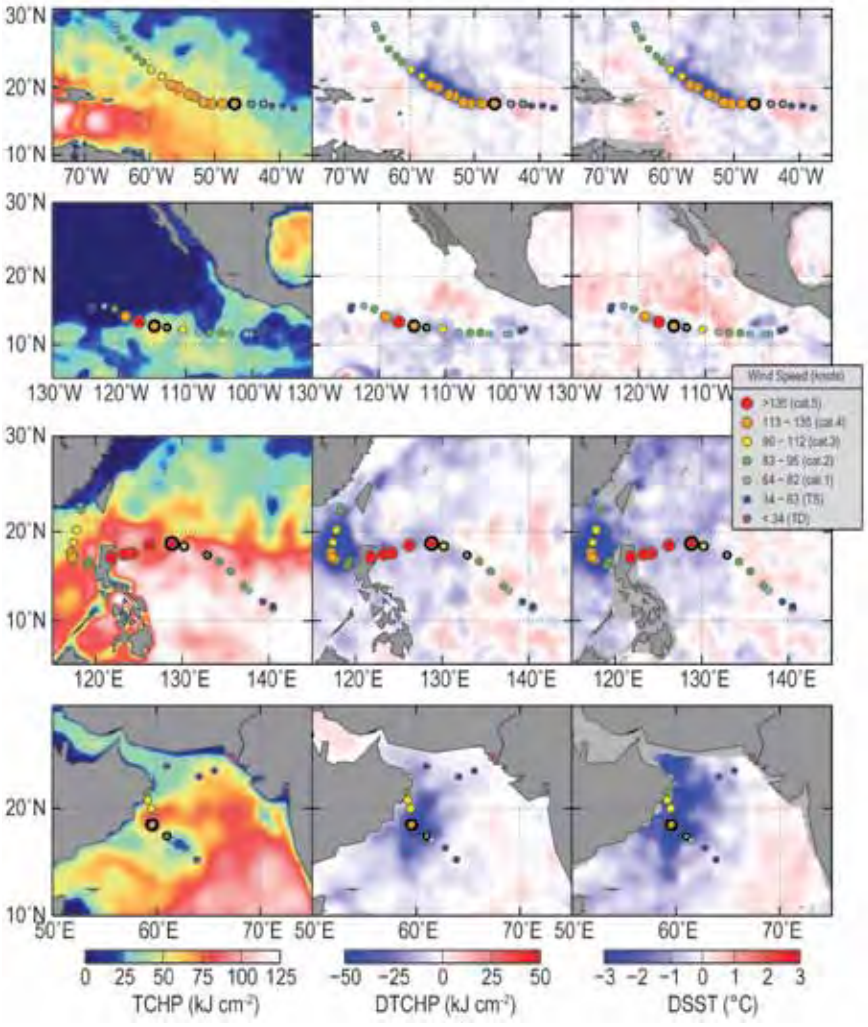

Fig. 4.29. (left) Tropical Cyclone Heat Potential (TCHP) and surface cooling given by the difference between post and pre storm values of (center) tropical cyclone heat potential and (right) sea surface temperature, for (from top to bottom) Hurricane Igor, Hurricane Celia, Typhoon Megi, and Cyclone Phet.

values of up to 50 kJ cm^{-2} in TCHP and above 3°C in SST, is important since these factors influence the upper ocean thermal structure on regional scales within weeks to months after the passage of the storms (Emanuel 2001; Hart et al. 2007).

In the Atlantic, preliminary best track estimates show Igor intensifying from 65 kts (33 m s^{-1}) to 130 kts (67 m s^{-1}) in 24 hours while the TC slowed down and the environmental vertical wind shear conditions improved. Values of TCHP under the track of this TC during this time also increased to values greater than 70 kJ cm^{-2}, well above the 50 kJ cm^{-2} usually found in cases of Atlantic rapid intensification (Mainelli et al. 2008). The post-storm surface cooling associated with the wake of this hurricane reached very high values, of approximately 5°C and 50 kJ cm^{-2}.

In the ENP, both Major Hurricanes Celia and Darby occurred in late June and showed peak intensity nearly coincident with positive TCHP anomalies. Celia formed on 18 June, southeast of Acapulco, Mexico, and on 24 June, with appropriately favorable atmospheric conditions given by the weakening of the shear, this cyclone rapidly intensified and gained its peak strength with winds of 140 kts (72 m s^{-1}). This intensification occurred when Celia traveled over a warm eddy containing waters with increased TCHP values which were close to 65 kJ cm^{-2}. The cooling under the track of this TC was weaker than Igor in the Atlantic Ocean, with observed SST values near 3°C and TCHP of 30 kJ cm^{-2}. This weaker oceanic response may be a response to the generally stronger vertical stratification found in the eastern Pacific that makes the ocean more difficult to mix. Despite the higher anomaly values of TCHP in the WNP, the season was a record-low year of TC occurrence. Despite the small number of observed storms, the TCHP conditions in September and October 2010 were extraordinarily favorable in the WNP, especially to the west of 150°E and to the south of 20°N, with values ranging from 120 kJ cm^{-2} to 170 kJ cm^{-2}, which are values well above the TCHP values commonly observed for super typhoons in this region (Lin et al. 2008, 2009).

As compared to the conditions in 2009, 2010 TCHP values were significantly greater by approximately 20 kJ cm^{-2} to 50 kJ cm^{-2} (Fig. 4.28). These unusually high TCHP values provided very favorable ocean conditions for the intensification of Super Typhoon Megi, the most intense TC globally in 2010. Megi formed to the west of Guam on 12 October 2010, and strengthened to a Category 5 super typhoon by 17 October. According to the preliminary Joint Typhoon

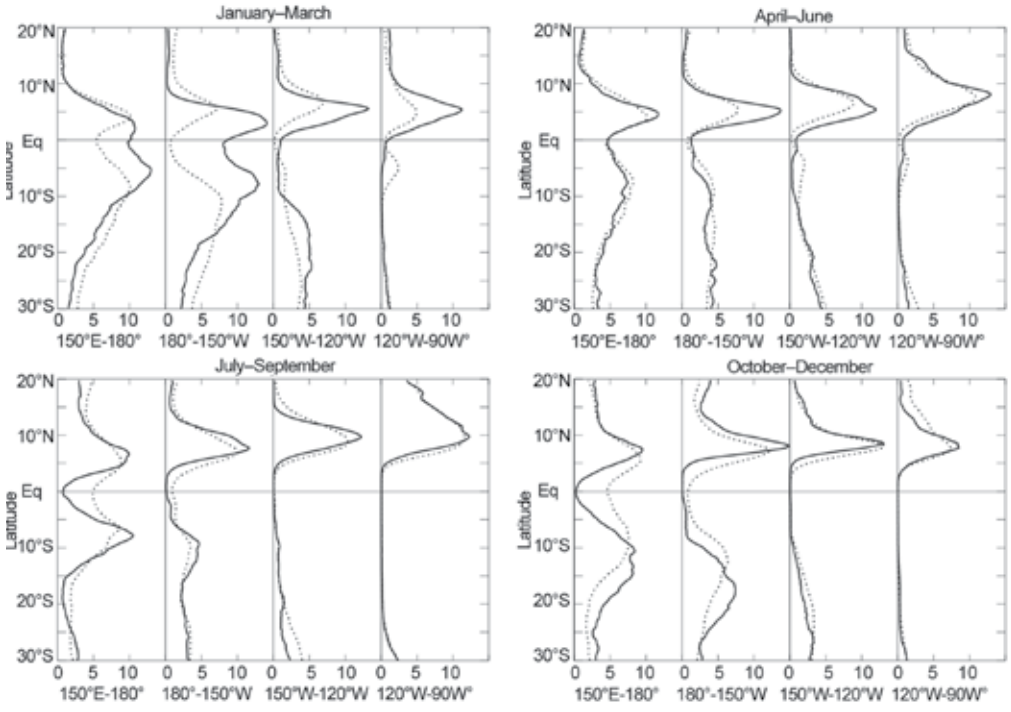

Fig. 4.30. Rainfall rate (mm day^{-1}) from TRMM 0.25° analysis for January–March, April–June, July–September, and October–December 2010. The separate panels for each three-month period show the 2010 rainfall cross-section between 20°N and 30°S (solid line) and the 1999–2008 climatology (dotted line), separately for four 30° sectors from 150°E–180° to 120°W–90°W.

of high TCHP of ~75 kJ cm^{-2}. After its departure from this high patch of TCHP, Phet weakened to approximately 105 kts (54 m s^{-1}) before making landfall in Oman, where it caused substantial damage estimated at ~$780 million (U.S. dollars) and accounted for 44 deaths. The storm later recurved over the northern Arabian Sea making a second landfall near the India-Pakistan border.

Warning Center (JTWC) report, Megi's intensity reached 160 kts (82 m s^{-1}), and an aircraft estimated its central pressure at 885 hPa, which is among the lowest TC pressures ever observed. Megi developed in this very favorable warm pool (Fig. 4.29) of extremely high TCHP values (typically ~100 kJ cm^{-2}–130 kJ cm^{-2}) throughout its genesis and intensification period. From 14 to 17 October, Megi intensified from a named storm to a Category 5 TC with maximum sustained winds of 160 kts (82 m s^{-1}). Megi subsequently made landfall in the Philippines.

Cyclone Phet was the most intense TC in the Arabian Sea in 2010 (Fig 4.29). The disturbance that eventually became Phet was identified early on 30 May and upgraded to a named storm on 31 May after a short genesis period. Early on 1 June, the moderate vertical wind shear relaxed and Phet intensified to a Category 1 cyclone with maximum sustained winds estimated at 65 kts (33 m s^{-1}) by JTWC. In the next 18 hours, it rapidly intensified from 65 kts (33 m s^{-1}) to 125 kts (64 m s^{-1}) to its peak at Category 4, an astonishing intensification rate well above the criteria for rapid intensification of 30 kts (15 m s^{-1}) in 24 hours (Kaplan and DeMaria 2003). The period of rapid intensification took place as Phet entered into a region

f. Intertropical Convergence Zones

1) Pacific—A. B. Mullan

This discussion for the Pacific sector covers the two prominent convergence zones: the Intertropical Convergence Zone (ITCZ) in the Northern Hemisphere, which lies approximately parallel to the Equator with a slight poleward tilt on its eastern end, and varying in position from around 5°N–7°N in February–May to 7°N–10°N in August–November; and the South Pacific Convergence Zone (SPCZ), which extends diagonally from around the Solomon Islands (10°S, 160°E) to near 30°S, 140°W, and is most active during November–April.

The behavior of the Pacific convergence zones in 2010 is readily characterized in two parts, with the first half of the year dominated by El Niño and the second half by La Niña. Thus, in the first half of 2010, both the ITCZ and SPCZ tended to be further equatorward than usual, with well-above-normal rainfall east of the date line near the Equator. In the second half of 2010, both the ITCZ and SPCZ tended to be poleward of their normal positions, with a much enhanced dry zone along the Equator. Figure 4.30 shows quarterly rainfall in the Pacific along transects from 20°N to 30°S, as derived from the 0.25°-resolution

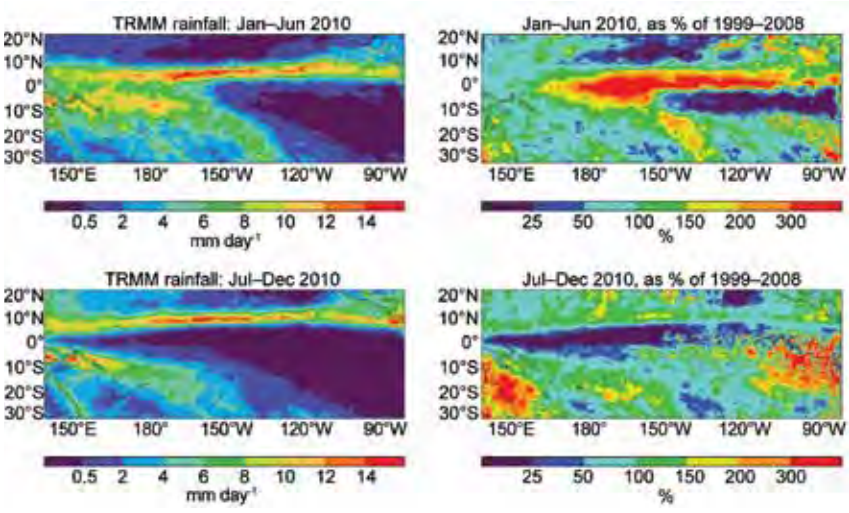

Fig. 4.31. Average rainfall rate (mm day^{-1}) from TRMM 0.25-degree analysis for January–June 2010 and July–December 2010, left-hand panels; and percentage anomaly from the 1999–2008 average, right-hand panels.

NASA TRMM rainfall data (3B-43 product; Huffman et al. 2007). The transects are broken up into four longitude sectors, depicting how the peak rainfall shifts poleward in each hemisphere as one progresses eastward across the Pacific. The 2010 positions of the convergence zones are compared with the 10-year climatology from 1999 to 2008.

The year began with a significant El Niño present in the Pacific. Although sea surface temperature anomalies decreased progressively from their peak in November–December 2009, temperatures remained at least 0.5°C above average through April 2010 and were sufficient to support enhanced deep tropical convection. Figure 4.30 shows substantially higher-than-normal rainfall in the first quarter of 2010 between 5°N–7°N and 10°S. Island groups within this band experienced wet conditions, with the month of February being particularly extreme; Christmas Island in eastern Kiribati (approximately 2°N, 157°W) recorded a new record rainfall for February with 818 mm, and Penrhyn in the Northern Cooks (10°S, 158°W) recorded a new February record of 1033 mm (ICU 2010).

Conversely, with the ITCZ contracting towards the Equator, islands north of about 7°N experienced dry conditions in the first half of the year. The Marshall Islands and Micronesia (around 7°N–10°N in the 150°E–180° sector, Fig. 4.30) were affected, as was Hawaii (near 20°N in the 180°–150°W sector); according to PEAC (2010), the Hawaiian wet season of October 2009 to April 2010 was the driest in the past 30 years. One convergence zone feature not present during 2010 was a double ITCZ, whereby a southern branch of the ITCZ appears in austral fall in the eastern tropical Pacific. Circulation and surface flux anomalies prevent this occurring in El Niño years (Masunaga and L'Ecuyer 2010), so it was not surprising to find the double ITCZ absent in 2010 (Fig. 4.31, top panels).

By July 2010, La Niña conditions were established across the Pacific and the climatic and circulation anomalies intensified further during the last quarter of the year. The peak rainfalls in the centers of the convergence zones were not markedly different from average, even on a monthly basis. However, both the ITCZ and SPCZ were shifted polewards and this had consequences for some island groups; the Fiji Islands (near the date line at 20°S) experienced wet

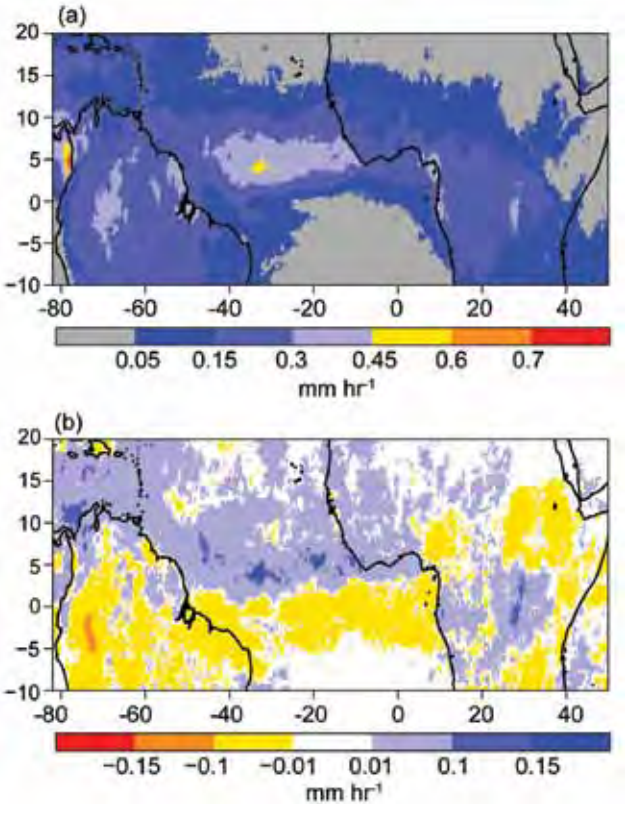

Fig. 4.32. TRMM (a) mean and (b) anomalous precipitation rate (mm hr^{-1}) for 2010. The anomaly was calculated based on the climatology for the period 1998–2009.

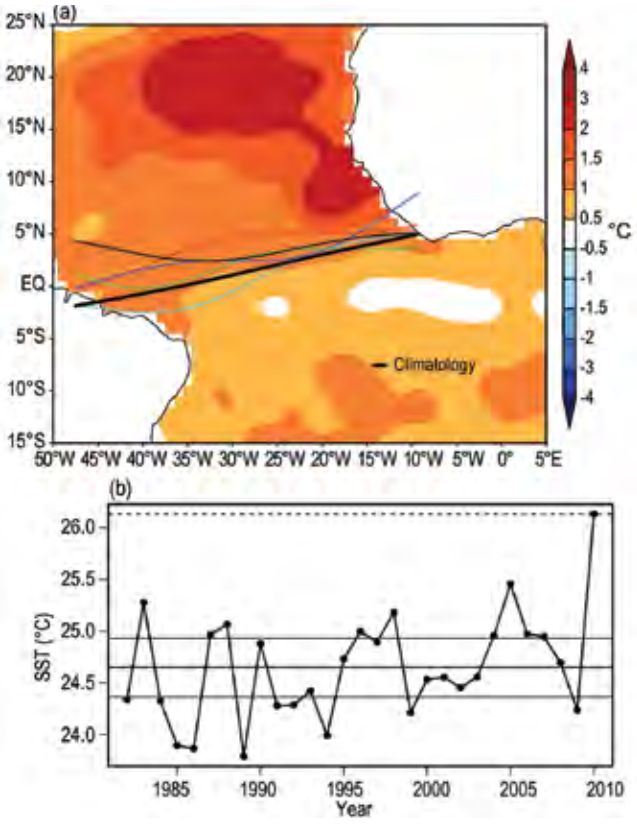

Fig. 4.33. (a) Atlantic Intertropical Convergence Zone (ITCZ) position inferred from outgoing longwave radiation during April 2010. The colored thin lines indicate the approximate position for the six pentads of April 2010. The black thick line indicates the Atlantic ITCZ climatological position. The sea surface temperature (SST) anomalies (Reynolds et al. 2002) for April 2010 based on the 1982–2009 climatology are shaded; and (b) April SST time series averaged over the tropical coast of northern Africa (20°E–50°E, 5°N–25°N) for the period 1982–2010. The solid horizontal central line indicates the long-term mean (climatology) of 24.6°C. The other two solid horizontal lines represent the upper and lower terciles of 24.9°C and 24.4°C, respectively. The dashed horizontal line puts the record value of 26.1°C measured in April 2010 in climate perspective.

conditions in the last quarter, as for the most part did New Caledonia on the eastern edge of the Coral Sea. More remarkable was the intensity of the dry zone along the Equator, which extended westwards of 150°E (Fig 4.31). The second panel in the October–December TRMM rainfall transects (Fig. 4.30) indicates almost no rainfall between about 5°N and 7°S east of the date line; in a major turnabout from February, Christmas Island (eastern Kiribati) received less than 10 mm in November, while in the same month Penrhyn (Northern Cooks) had only about 25% of its normal November rainfall.

2) Atlantic—A. B. Pezza and C. A. S. Coelho

(i) Description

The Atlantic ITCZ is a well organized convective band that oscillates approximately between 5°N–12°N during July–November and 5°N–5°S during January–May (Waliser and Gautier 1993; Nobre and Shukla 1996). Equatorial Kelvin waves can modulate the ITCZ interannual variability and ENSO is also known to influence the ITCZ on the seasonal time scale (Münnich and Neelin 2005). In 2010, the Atlantic ITCZ presented an anomalous displacement to the north of its normal position, indirectly contributing to a severe drought in the Amazon and northeastern Brazil (Fig. 4.32 and Fig. 4.33a). As a result, adverse impacts were felt on cargo and human transportation that rely on local rivers in the Amazon. Conversely, the ITCZ was also directly associated with above-average precipitation on the western tropical coast of Africa between 5°N and 20°N (Fig. 4.32b).

Although the year was highlighted by the onset of a moderate-to-strong La Niña beginning in July, with global climate anomalies typical of a positive Southern Oscillation Index (SOI) regime arising in many areas of the globe, it was the Atlantic SST gradient between the Northern and the Southern Hemispheres that played a fundamental role in explaining the anomalous behavior of the Atlantic ITCZ in 2010 (Fig. 4.33a). Since January, the Atlantic remained anomalously warm to the north of the Equator, reaching satellite-era record warming conditions of 26.1°C towards April (Fig. 4.33b). This record warming is

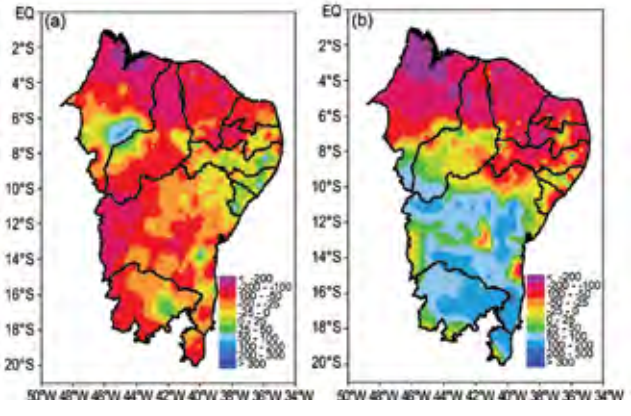

Fig. 4.34. Northeastern Brazil precipitation anomalies (mm) during (a) February and (b) March 2010 with respect to 1961–90 climatology based on high resolution station data. [Data source: several federal and regional networks based in Brazil (e.g., CMCD/INPE, INMET, SUDENE, ANEEL, FUNCEME/CE, LMRS/PB, EMPARN/RN, LAMEPE/ITEP/PE, CMRH/SE, SEAAB/PI, SRH/BA, CEMIG/SIMGE/MG, SEAG/ES)].

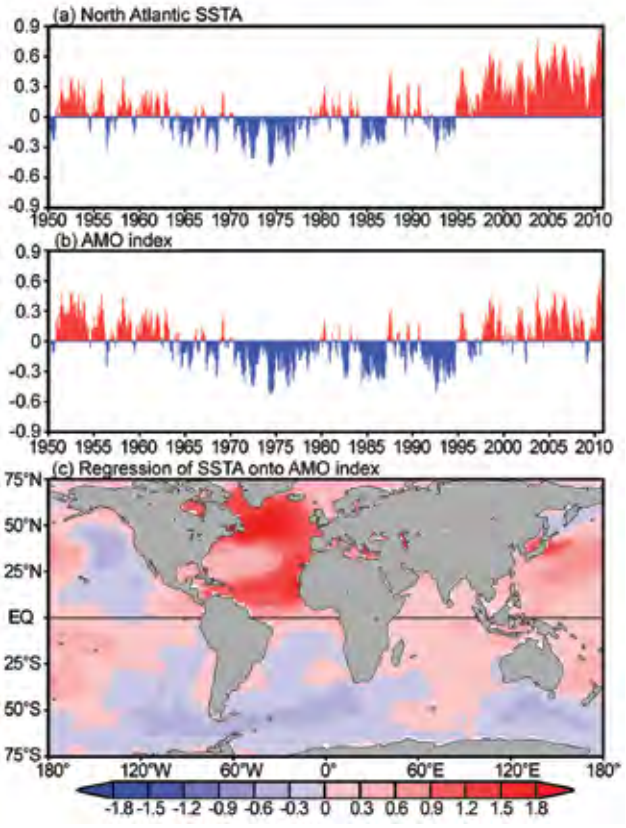

Fig. 4.35. The index of the Atlantic Multidecadal Oscillation (AMO) and its spatial pattern. Shown are: (a) the sea surface temperature (SST) anomalies (°C) in the North Atlantic for 0°–60°N and from the east coast of the Americas to 0° longitude; (b) the AMO index (°C) defined by the detrended (removing the linear trend) North Atlantic SST anomalies; and (c) regression (°C per °C) of global SST anomalies onto the AMO index of (b). The monthly SST anomalies are calculated as departures from the 1971–2000 climatology.

remarkable as it encompassed a very large area of the North Atlantic, and is more than 0.6°C above the second largest value of 25.5° C recorded in April 2005 in this region. The warming persisted throughout most of the year, losing intensity only in November, while La Niña conditions remained moderate-to-strong.

As a result, the ITCZ did not exert a significant contribution towards the rain in northeastern Brazil in 2010, with a large portion of the region experiencing much drier conditions than average, especially in February and March when the climatological influence of the ITCZ towards the Southern Hemisphere should have been important (Fig. 4.34).

g. Atlantic Multidecadal Oscillation—C. Wang

The Atlantic Multidecadal Oscillation (AMO) is an oscillatory mode defined by the detrended North Atlantic SST anomalies over the region of 0°–60°N and from the east coast of the Americas to 0° longitude (Figs. 4.35a,b; Delworth and Mann 2000; Enfield et al. 2001; Wang et al. 2008a; see also Sidebar 1.1). A driving mechanism for the AMO is the Atlantic meridional overturning circulation (Delworth and Mann 2000; Knight et al. 2005; Dijkstra et al. 2006; Zhang et al. 2007; see also section 3h for detailed information on the meridional overturning circulation). The AMO demonstrates an interannual variation via its connection to the tropical Atlantic Warm Pool (AWP; a large body of warm water comprising the Gulf of Mexico, Caribbean Sea, and the western tropical North Atlantic), and as such has exhibited a seasonal influence on the behavior of tropical cyclones (TCs) in the Atlantic and Eastern North Pacific (ENP) basins. The extended reconstructed SST (ERSST) data from 1950 to 2010 shows that the AMO was in the cold phase from the late 1960s to the early 1990s and in the warm phase before the late 1960s and again, after the early 1990s. The AMO is related to SST anomalies over the global oceans as shown in Fig. 4.35c.

The AMO variability is associated with changes of climate and extreme events, such as drought and flood in North America and Europe, and Atlantic hurricane activity (Enfield et al. 2001; McCabe et al. 2004; Goldenberg et al. 2001; Bell and Chelliah 2006; Wang et al. 2008a). Recent studies show that the importance of the AMO is due to its tropical component since the climate response to the North Atlantic SST anomalies is primarily forced at the low latitudes (Sutton and Hodson 2007; Wang et al. 2008b). Since the AWP is at the center of the main development region (MDR) for Atlantic tropical cyclones, the influence of the AMO on climate and Atlantic TC activity operates through the mechanism of the AWP-induced atmospheric changes by having an effect on vertical wind shear in the MDR. A large AWP reduces such shear, while a small AWP enhances it. A large AWP also weakens the southerly Great Plains low-level jet, thus reducing the northward moisture transport from the Gulf of Mexico to the eastern U.S. and decreasing the boreal summer rainfall over the central U.S., while a small AWP has the opposite effect (Wang et al. 2006; Wang et al. 2008b). It has also been shown that AWP variability can produce the observed out-of-phase relationship between TC activity in the tropical North Atlantic and ENP (Wang and Lee 2009).

The AMO in 2010 remained in its warm phase and showed extremely positive SST anomalies in the North Atlantic (Fig. 4.36a). The warm phase of the AMO was strongest in August (+0.90°C) and weakest

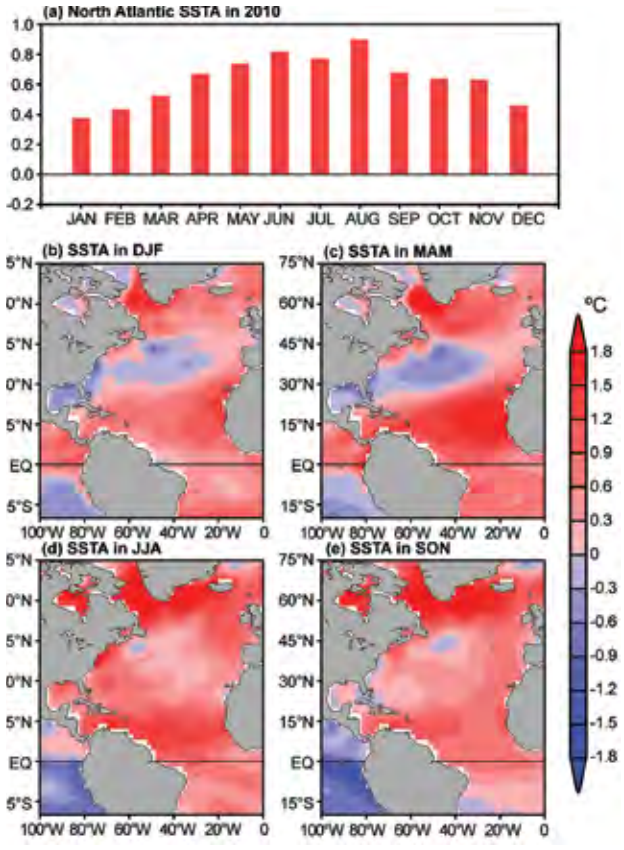

Fig. 4.36. The Atlantic Multidecadal Oscillation (AMO) in 2010. Shown are: (a) the monthly North Atlantic sea surface temperatures (SST) anomalies (°C) in 2010; (b) the DJF (December 2009–February 2010) SST anomalies (°C); (c) the MAM (March–May 2010) SST anomalies; (d) the JJA (June–August 2010) SST anomalies; and (e) the SON (September–November 2010) SST anomalies. The monthly SST anomalies are calculated as departures from the 1971–2000 climatology.

in January (+0.38°C). Spatially, the North Atlantic SST anomalies during the boreal winter and spring seasons showed a tripole pattern with the positive SST anomalies in the subpolar North Atlantic and the tropical North Atlantic and the negative SST anomalies in the subtropical North Atlantic (Figs. 4.36b,c). The SST anomaly pattern divided the AWP into two parts: a colder Gulf of Mexico and a warmer Caribbean Sea/western tropical North Atlantic. The opposite SST anomaly pattern was consistent with a previous study (Muñoz et al. 2010), which showed that the air-sea fluxes associated with ENSO events in the tropical Pacific and local processes were responsible for the SST anomaly distribution.

During the boreal summer and fall of 2010, the cold SST anomalies in the subtropical North Atlantic almost disappeared and the North Atlantic was consistently warm (Figs. 4.36d,e). During the 2010 Atlantic TC season, the AWP was also consistently large and the entire tropical North Atlantic was warm. A large AWP also tends to shrink the North Atlantic subtropical high eastward (C. Wang et al. 2007) and hurricanes are therefore steered away from the eastern coast of the United States. The extremely large AWP in 2010 was also associated with the out-of-phase relationship between TCs in the North Atlantic and the ENP as documented in sections 4d2 and 4d3.

h. Indian Ocean Dipole—J. J. Luo

Year-to-year climate variability in the tropical Indian Ocean (IO) is largely driven by local ocean-atmosphere interactions and ENSO. The Indian Ocean Dipole (IOD), as one major internal climate mode in the IO, may sometimes be originated from complex interactions between the IO and Pacific (J.-J. Luo et al. 2010). Owing to the warm mean state in the IO, the IOD often causes large climate anomalies in many countries surrounding the IO despite the fact that SST anomalies related to IOD are usually weak and more localized compared to the ENSO signal. During late boreal summer to fall in 2010, a negative IOD (nIOD) occurred, five years after the last nIOD event in 2005 (Luo et al. 2007). Compared to previous events, the 2010 nIOD was strong, with a peak warming of about 1°C above normal in the eastern IO (Fig. 4.37b) during 2010 fall season; this event may have

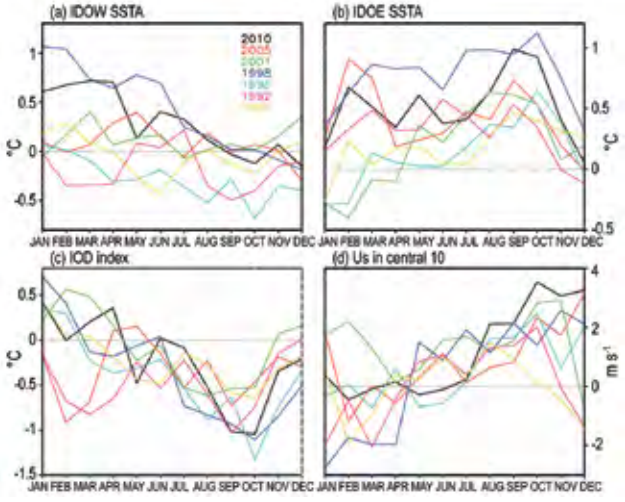

Fig. 4.37. Monthly anomalies of (a) sea surface temperatures (SST) in the western Indian Ocean (IODW, 50°E–70°E, 10°S–10°N); (b) SST in the eastern IO (IODE, 90°E–110°E, 10°S–0°); (c) the IOD index (measured by the SST difference between IODW and IODE) during the seven negative IOD events; and (d), as in (c), but for the surface zonal wind anomaly in the central equatorial IO (70°E–90°E, 5°S–5°N).

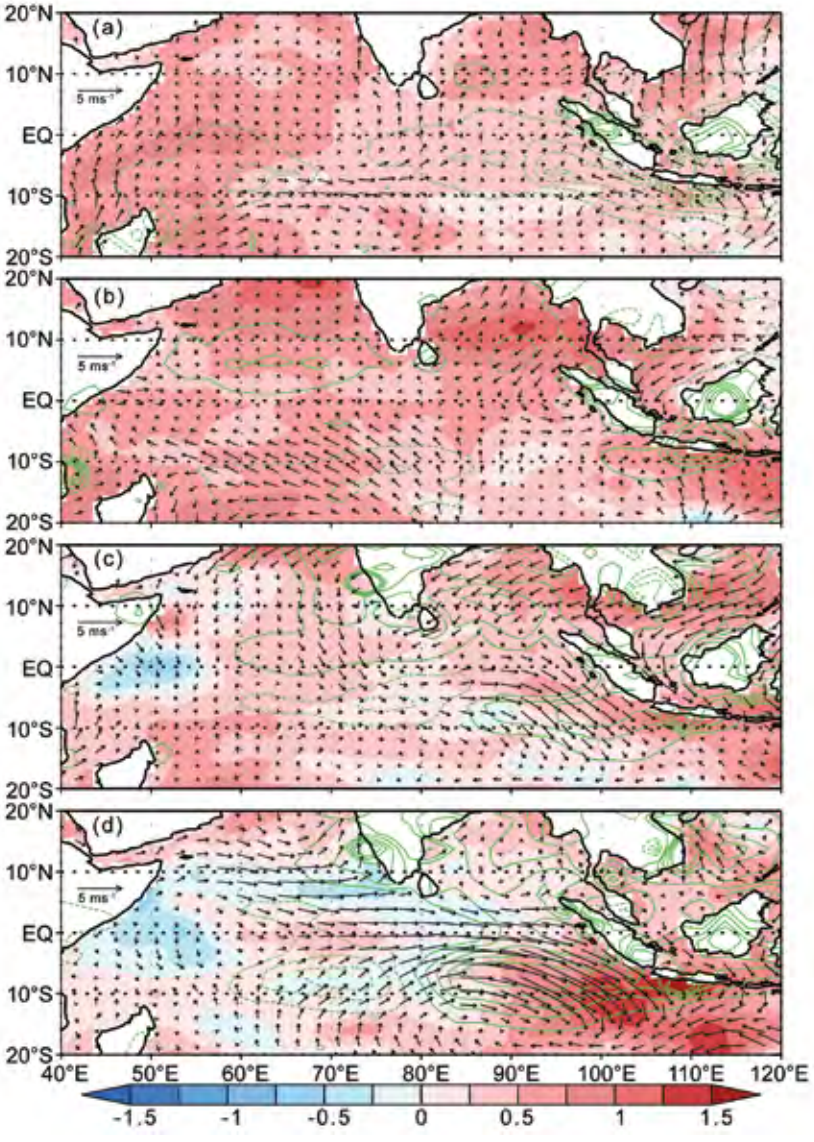

Fig. 4.38. Sea surface temperature (°C, colored scale), precipitation (green contour: ±1, ±2, …,±5 mm day^{-1}), and surface wind anomalies during (a) December–February 2009/10; (b) March–May 2010; (c) June–August 2010; and (d) September–November 2010. Anomalies were calculated relative to the climatology over the period 1982–2009. These are based on the NCEP optimum interpolation SST (Reynolds and Chelton 2010), monthly GPCP precipitation analysis (http://precip.gsfc.nasa.gov/), and JRA-25 atmospheric reanalysis (Onogi et al. 2007).

contributed to the floods in Indonesia and Australia.

Sea surface temperatures in major parts of the tropical IO during early 2010 were warmer than normal in association with influence of the strong El Niño, which peaked in December 2009 (Fig. 4.38a). This El Niño caused basin-wide drought in the IO; as a result, more surface solar radiation and less latent heat loss contributed to the IO basin-wide warming. Large warming appeared in the western IO mainly due to the surface heat flux forcing, whereas local subsurface temperature was below normal. The warming contrast between the western and eastern IO led to a weak positive IOD index during January–April 2010 (black line in Fig. 4.37c). In March–May 2010, the IO basin-wide warming persisted (Fig. 4.38b) despite the rapid weakening of the El Niño signal; this represents the well-known delayed impact of ENSO on the IO climate. Large warming appeared in the North IO and Indonesia-Australia area. The latter warming induced surface convergence and hence more rainfall along the south coast of Java. Correspondingly, a local northwesterly anomaly occurred along the west coast of Sumatra and persisted until July 2010 (Figs. 4.37d, and 4.38b,c). It is interesting to note that the IOD index in May 2010 reached about -0.5°C because of the sudden decrease (increase) of the western (eastern) IO SST anomalies (black lines in Figs. 4.37a–c). This monthly fluctuation, however, was not coupled with the surface wind anomaly in the central IO (Fig. 4.37d); it appears to have been induced by intraseasonal oscillations in the IO.

Massive westerly anomalies in the equatorial IO appeared in August 2010; this is related to the impact of a moderate-to-strong La Niña, which had developed quickly in mid-2010. The westerly anomalies in the central IO drove a downwelling oceanic Kelvin wave, which subsequently propagated eastward and deepened the thermocline along the west coast of Sumatra (Fig. 4.39a). As a result, the original warming near the Java coast intensified and expanded northward, and strong northwesterly anomalies occurred along the west coast of Sumatra during late summer to fall in 2010 (Figs. 4.38c,d). Meanwhile, SSTs in the western IO decreased due to both La Nina's influence and nIOD development. The warming (cooling) of SST in the east (west) and

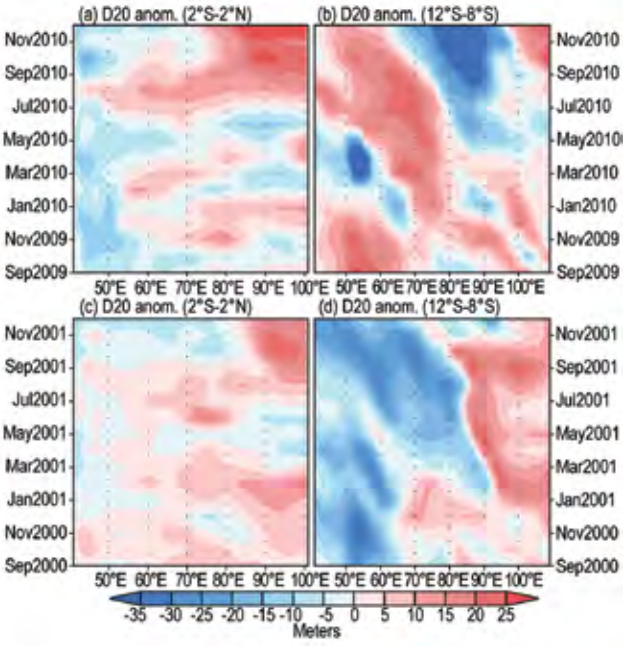

Fig. 4.39. 20°C isotherm depth (D20, meter) anomalies in (a) the equatorial Indian Ocean (2°S–2°N) and (b) off-equatorial South Indian Ocean (12°S–8°S) associated with the negative Indian Ocean Dipole (nIOD) development in 2010. (c) and (d), as in (a) and (b), respectively, but for the D20 anomalies related to the nIOD event in 2001. Data are derived from the NCEP ocean reanalysis (http:/www.cpc.ncep.noaa.gov/products/GODAS/).

strengthening of the central IO westerly winds clearly represents the air-sea coupled process related to the nIOD growth. During November–December 2010, the nIOD signal weakened rapidly despite the strong westerly anomaly in the central IO (black lines in Fig. 4.37); this is due to the demise of warm SST anomalies in the eastern IO owing to the reversal of monsoonal winds. The stronger-than-normal winds and greater cloud coverage in the east weakened the SST warming in that region quickly.

The evolution of the nIOD in 2010 is similar to that of previous events (Fig. 4.37). Although significant variability among the seven nIOD events over the past two to three decades can be seen, the IOD index in most cases shows a positive value in early year, the onset in late spring to summer, the peak in fall, and the rapid demise in November–December (Fig. 4.37c). This is consistent with the strengthening of westerly winds in the central IO. While the western IO SST anomalies show a consistent decrease associated with the nIOD development, evolutions of SST anomalies in the eastern IO appear to be largely influenced by ENSO (Figs. 4.37a,b). In the four cases following El Niño events (1992, 1998, 2005, and 2010), warmer-than-normal SSTs in the eastern IO start to occur early in the year, persisting in spring and summer, and strengthening in fall. Contrasting this, in the three cases following La Niña events (1990, 1996, and 2001), SST anomalies early in the year were colder than normal or neutral. El Niño or La Niña events may also drive downwelling or upwelling oceanic Rossby waves propagating westward at about 10°S (Figs. 4.39b,d), which enhance or hamper the nIOD development in the following year. Therefore, it is possible that the nIOD event in 2010 may have been driven by both the previous El Niño and concurrent La Niña, but further research will be required to determine that more definitively.

SIDEBAR 4.1: EASTERN CANADA'S TROPICAL TAP—A RECORD YEAR FOR TROPICAL CYCLONE IMPACTS IN CANADA—C. T. FOGARTY AND H. J. DIAMOND

The 2010 Atlantic Hurricane Season was an active one, with 19 named storms and 12 hurricanes—five of which reached major hurricane status. The large-scale pressure patterns over the western North Atlantic Ocean and eastern North America permitted many of this year's tropical storms and hurricanes to track northward toward eastern Canada, leaving the United States relatively unscathed. Two storms directly affected Canada in 2010. On 4 September, the very large Hurricane Earl made landfall in Nova Scotia, followed on 21 September by Hurricane Igor walloping Newfoundland. Canada was also impacted by indirect effects from Tropical Storm Nicole and Hurricane Tomas in the form of flooding rains courtesy of a high-amplitude flow pattern over eastern North America.

Hurricane Earl arrived in Nova Scotia as one of the most well-defined hurricanes that forecasters here have seen in many years (Fig. 4.40). Earl made landfall as a 65 kt (33 m s^{-1}) Category 1 hurricane, resulting in a drowning fatality. Winds uprooted many trees, generated widespread power outages, and caused exterior damage to buildings. Significant wave heights of 10 meters to 13 meters were recorded with peak waves up to 23 meters, and storm surge in Bedford Basin (at the head of Halifax Harbor) reached 1.2 meters; however, the coastal surge and wave impacts were minimal since the hurricane arrived at low tide.

Hurricane Igor was by far the most damaging tropical cyclone to strike Newfoundland in the modern era with total damage estimates near $185 million (Canadian dollars). The combination of the hurricane and a front to its north (Fig. 4.41) caused severe river flooding over the entire eastern portion of the island of Newfoundland. Many bridges were washed away, leaving giant chasms in most major roads, resulting in a fatality and causing major disruptions for several weeks after the event. High winds blew roofs off homes on the Avalon Peninsula and toppled many trees in the capital city of St. John's. The proposal by the Meteorological Service of Canada to have the name Igor retired from the list of hurricane names was approved in May 2011. This is only the second Canadian hurricane whose name was retired from the list. Juan was removed from the list after striking Nova Scotia as a Category 2 hurricane in 2003, inflicting an estimated $200 million (Canadian dollars) worth of damage.

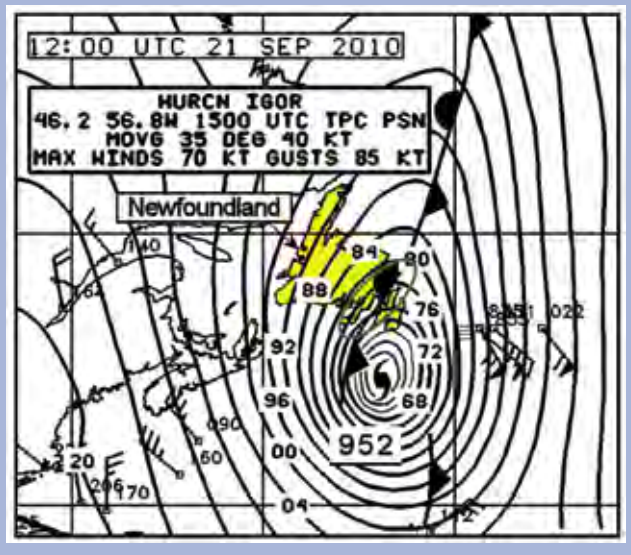

Fig. 4.41. Sea level pressure analysis of Hurricane Igor and large-scale pressure pattern with fronts at 12 UTC 21 September 2010. Image adopted from the NOAA Ocean Prediction Center. Area of extreme rainfall is shown by the green ellipse.

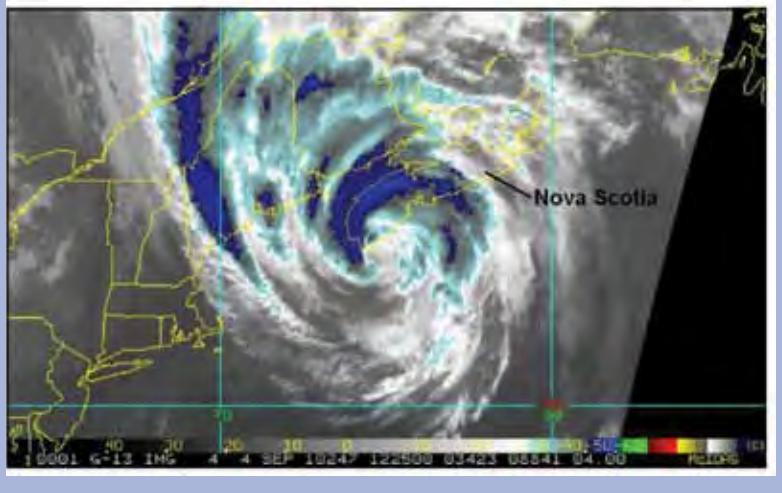

Fig. 4.40. Enhanced infrared satellite image of Hurricane Earl just before landfall in Nova Scotia at 1225 UTC 04 September 2010. Image courtesy of the NOAA/NESDIS tropical cyclone website at http://www.ssd.noaa.gov/PS/TROP/.

The moisture remnants of Tropical Storm Nicole (near Florida) swamped portions of southern Quebec, New Brunswick, and many U.S. states south of the Canadian border as a long front extended all the way from the province of Quebec to the remnant low associated with Nicole over the Bahamas. Two fatalities were reported in Canada from the heavy rainfall, which totaled almost 100 mm.

The tropical season's final assault on Canada was from the combined effects of

cont. SIDEBAR 4.1: EASTERN CANADA'S TROPICAL TAP—A RECORD YEAR FOR TROPICAL CYCLONE IMPACTS IN CANADA—C. T. FOGARTY AND H. J. DIAMOND

a dissipating Hurricane Tomas north of the Bahamas and a stationary belt of moisture streaming northward for several days (see Fig. 4.42). Similar to Nicole a little over a month earlier, a blocking pattern in the midlatitude flow was the culprit. A five-day deluge amounting to almost 300 mm caused major flooding over western Nova Scotia and southern New Brunswick. Some bridges were washed out and a number of homes were severely flooded. The example of Hurricane Tomas is very similar to a predecessor rain event as described by Galarneau et al. (2010).

The large-scale blocked weather pattern continued into December with four major marine storms pummeling eastern Canada in succession. Flood-weary New Brunswick was hit particularly hard with both ocean surge and freshwater flooding, marking the end of one of the stormiest spells of weather in recent memory for the region.

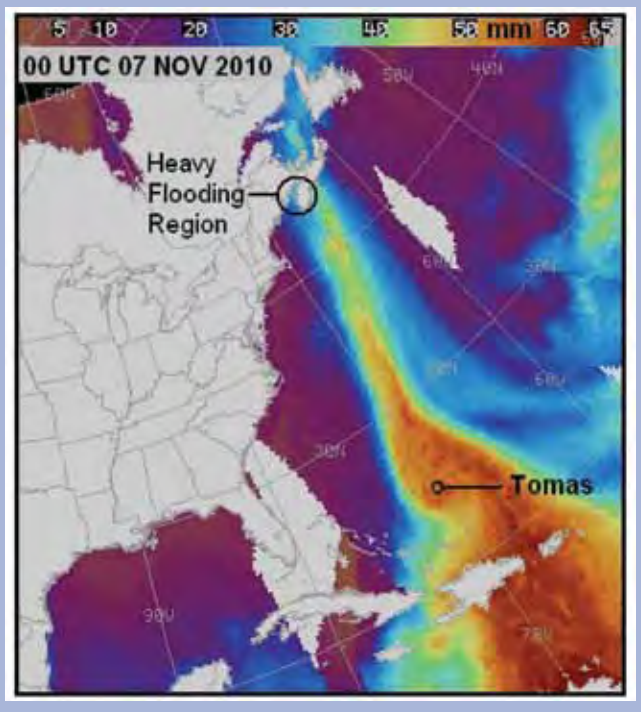

FIG. 4.42. Total column precipitable water at 00 UTC 07 November 2010 derived from the Special Sensor Microwave Imager (SSM/I) and Advanced Microwave Scanning Radiometer-Earth Observing System (AMSR-E) at the Cooperative Institute for Meteorological Satellite Studies (CIMSS).